附件七：李員於 4/8 PBNC 2016 英文簡報內容

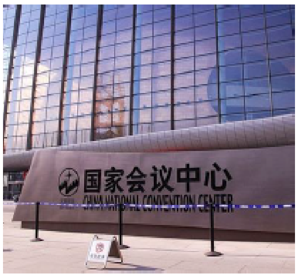

Associate Research Fellow
PO 3-27, Longtan
TEL/ 866-3-4711400
Ext.7165
E-mail/mhli@iner.gov.tw

An organic adsorbent resin for Ga-68 Generator

Ming-Hsin Li, 李銘忻

2016.04.08 北京 國家會議中心 PBNC.2016

Isotope Application Division
Institute of Nuclear Energy Research, Taiwan

Why need to develop Ga-68 generator ?

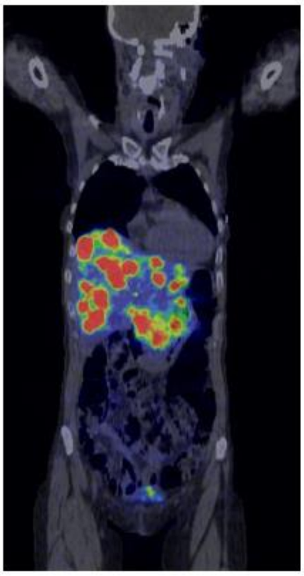

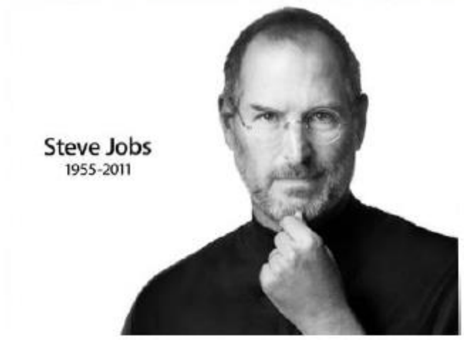

Steve Jobs cofounder and innovator of Apple Computer died on October 5, 2011 from complications of **pancreatic cancer**, he was 56 years old. Jobs made a huge impact on the culture of America with these techy gadgets that Americans absolutely love.

^{68}Ga-DOTATATE PET/CT, ^{99m}Tc-HYNIC-Octreotide SPECT/CT, and Whole-Body MR Imaging in Detection of Neuroendocrine Tumors: A Prospective Trial

J Nucl Med 2014; 55:1598–1604
DOI: 10.2967/jnumed.114.144543

Outline

- **Ga-68/Ge-68 Generator**
- **Our systematic innovation：**
  - Irradiation Product with Minimal Impurity
  - Method of Purification for Recycling of Ga-69 Isotope
  - The dual-core Ga-68 Radionuclide Generator
  - Automatic Synthesizer Apparatus for Producing Ga-68-DOTATATE
- **New drug application**

Why need to develop Ga-68 generator ?

Ga-68 will become the Tc-99m of PET/CT

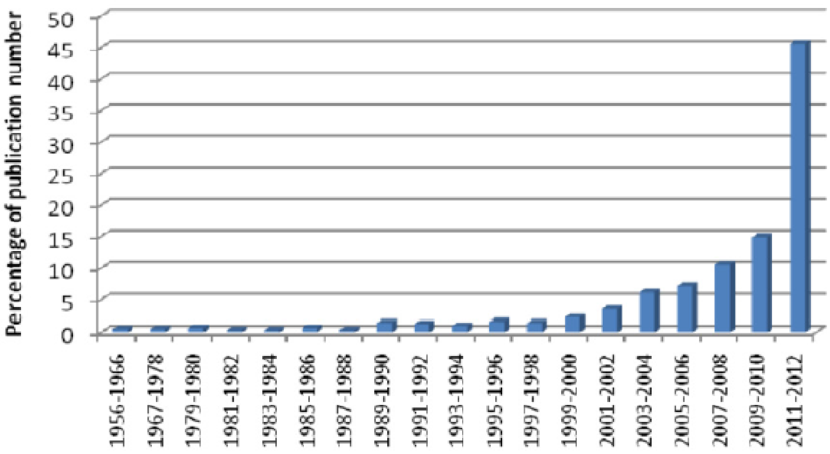

Use of ^{68}Ga as PET nuclide

Irina Velikyan (*Theranostics*, 2014)

^{68}Ga properties

- Physical properties
  - Halflife $T_{1/2}$ = 68 min
  - Positron branching 89% (PET nuclide)
  - Available via a ^{68}Ge/^{68}Ga generator
  - Mother ^{68}Ge cyclotron produced ($T_{1/2}$ = 271 d)
- Chemical properties of Ga
  - Trivalent metal
  - Chelation chemistry
- Applicability
  - Short half-life useful for molecules with fast biokinetics (Peptides, Ab-fragments, small complexes,…)

^{68}Ge/^{68}Ga generator.

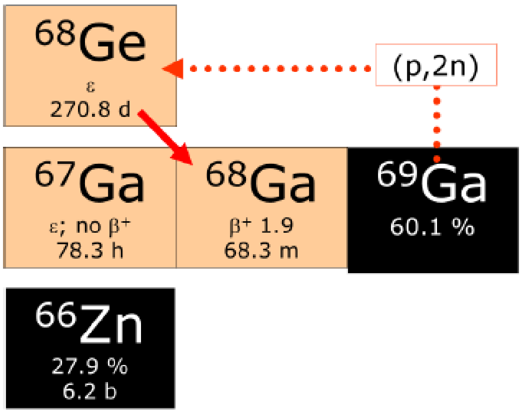

^{68}Ge/^{68}Ga generators --- currently in use

„Heidelberg" | ITG | Cyclotron/EZAG | EZAG | iThemba | IPL

Organic Matrix | *Titanium-dioxide* | *Tin-dioxide*

Elution

5.5N HCl | 0.05N HCl | 0.1N HCl | 0.1N HCl | 0.6-1N HCl | 1NHCl

and ……..?

An organic adsorbent resin for Ga-68 Generator

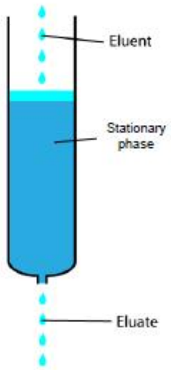

Process

Ga-68 eluent

↓

Filling with the organic resin (N-methylglucamine group)

↓

Ga-68 eluate (flow rate: 0.5 mL/min)

↓

Ge-68/Ga-68 generator

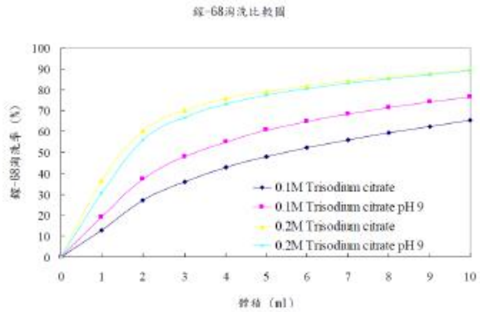

鎵-68-trisodium citrate 淘洗比較圖

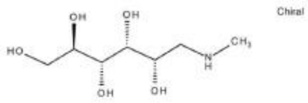

N-methylglucamine

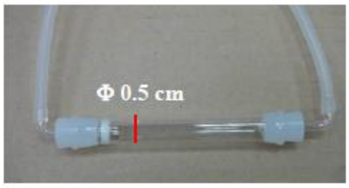

Scheme of ^{68}Ga Generator

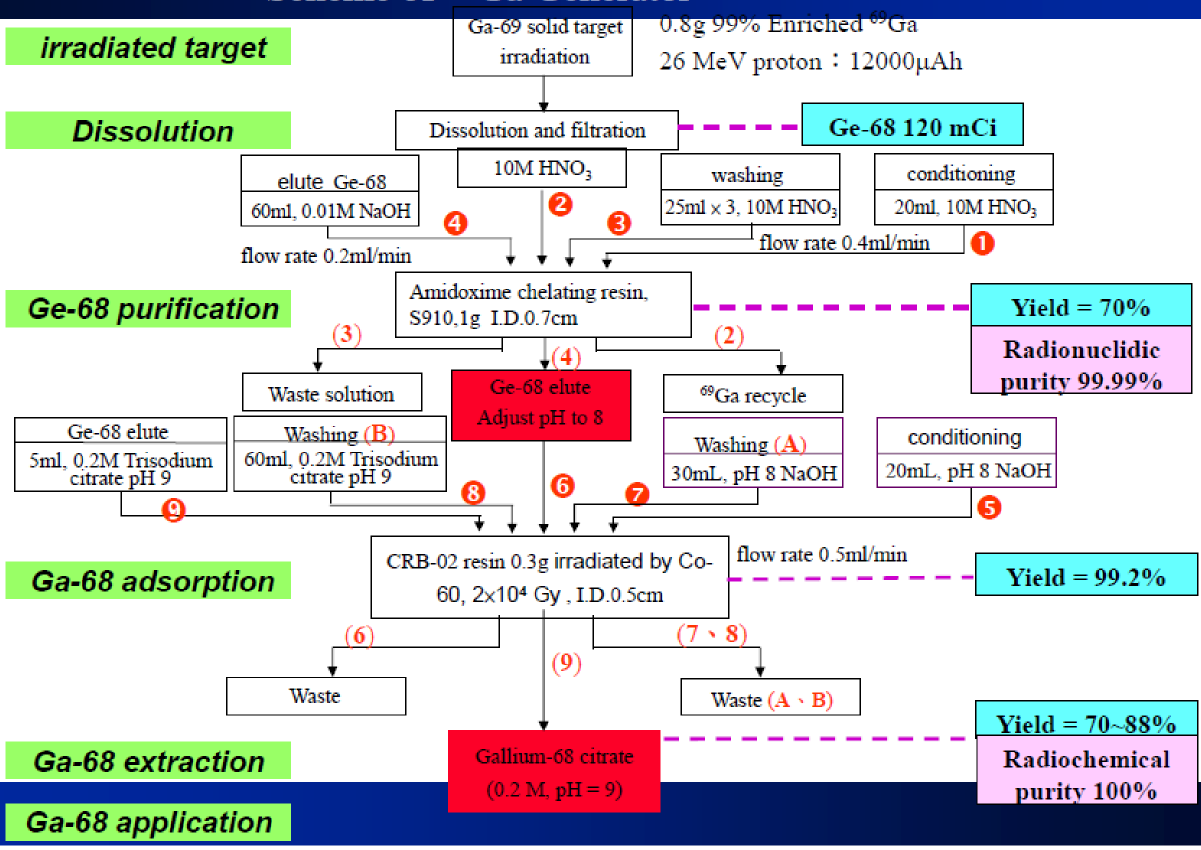

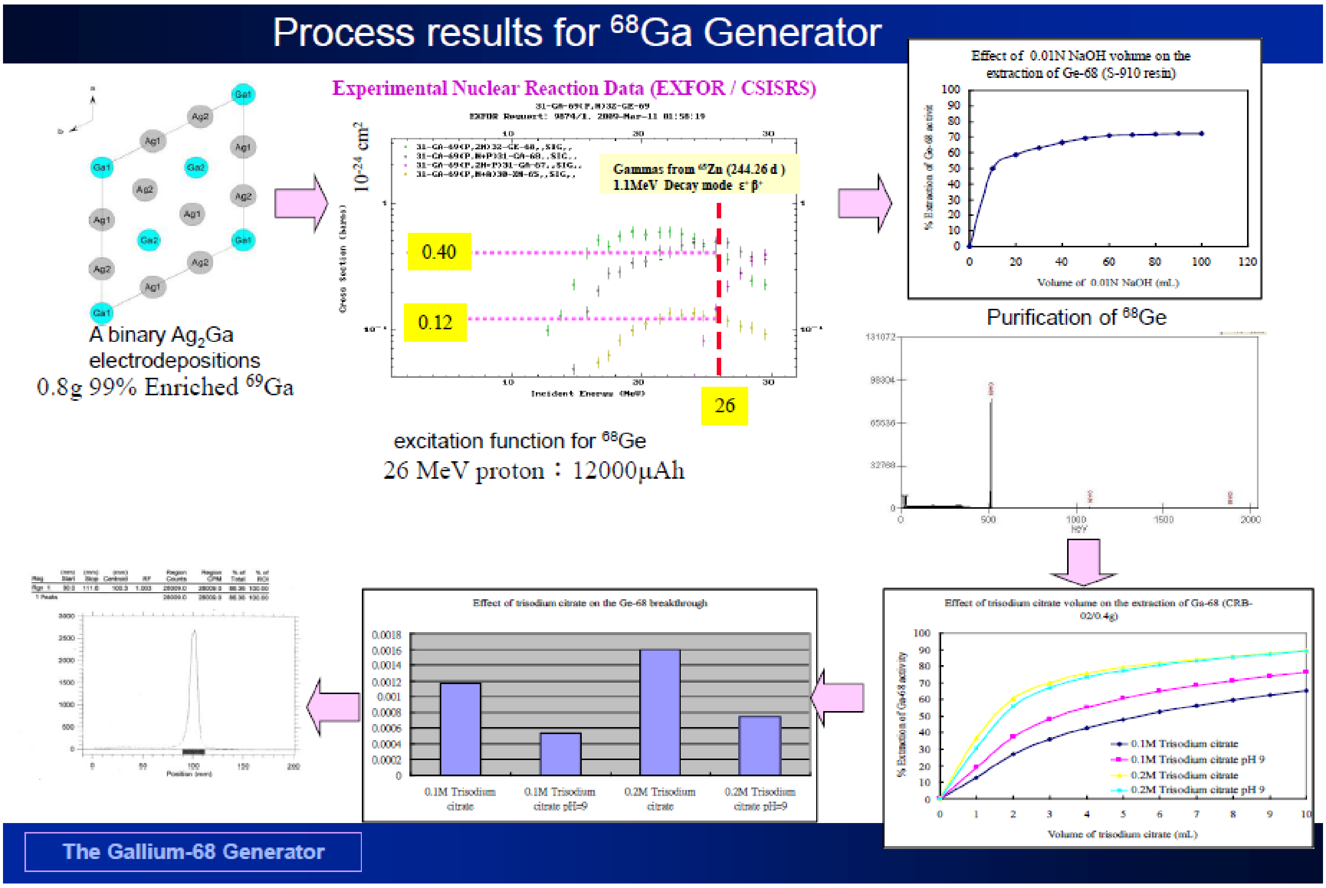

Quality control

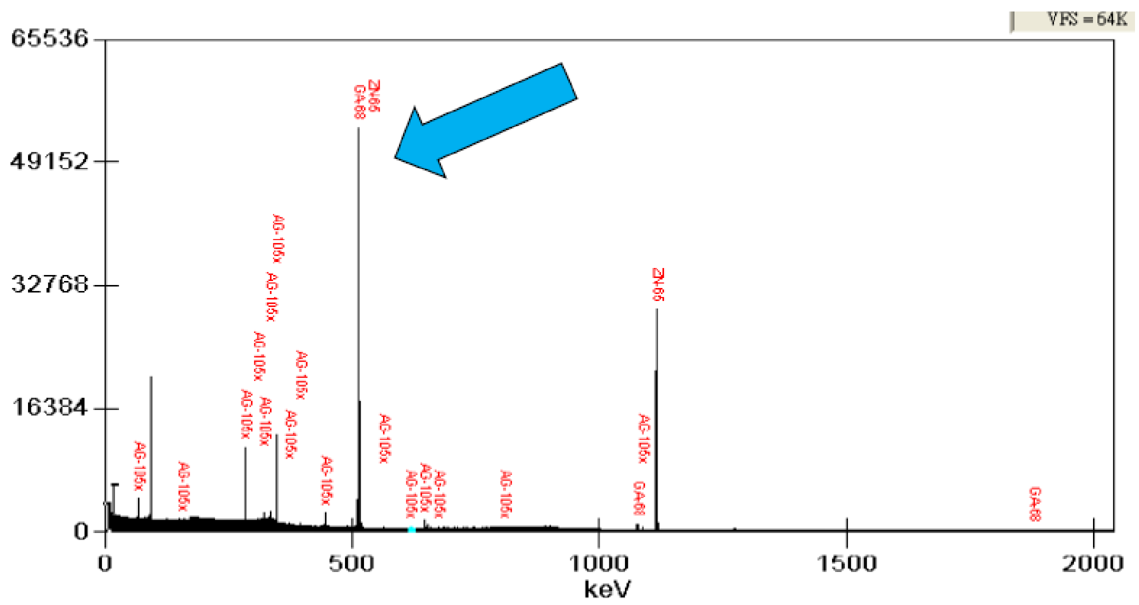

Figure of MCA spectrum for Radionuclide purity
After step I purification of S-910 resin

Quality control

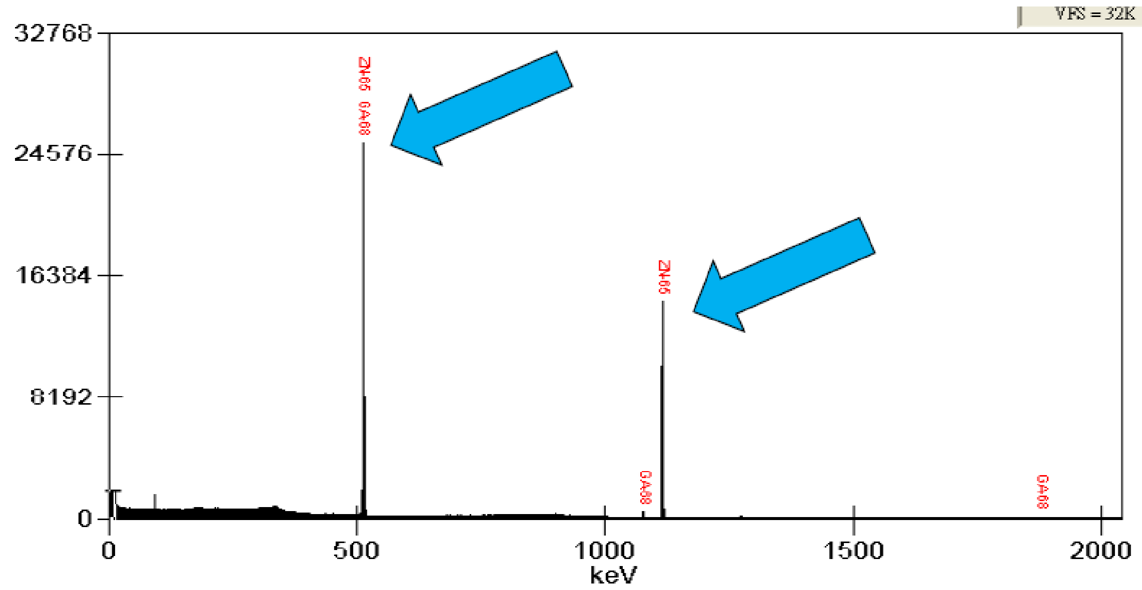

Figure of MCA spectrum for Radionuclide purity
After step II purification (S-910 resin with heated)

Quality control

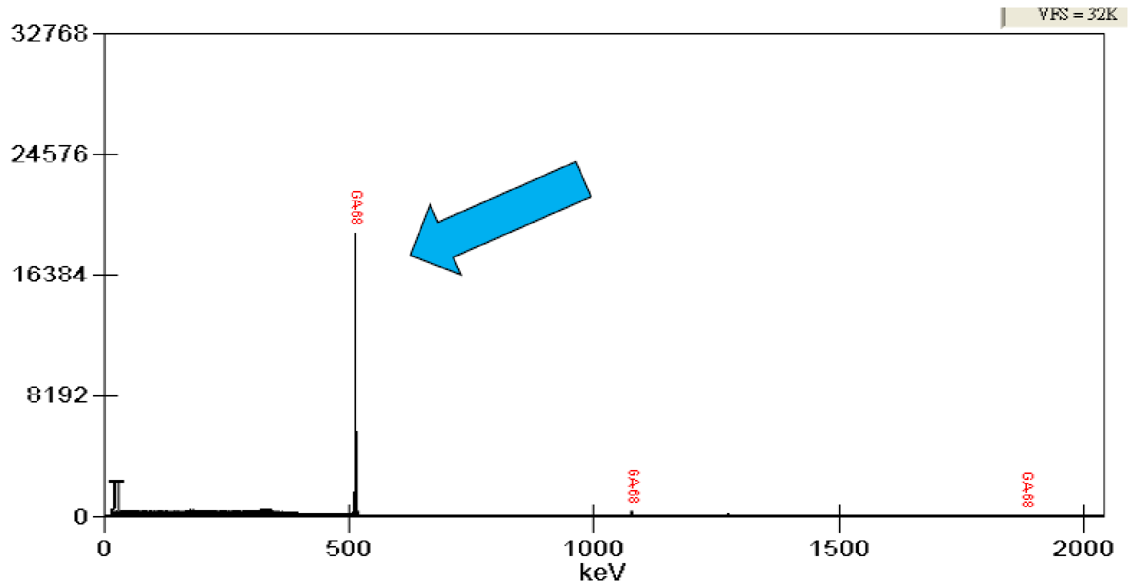

Figure of MCA spectrum for Radionuclide purity
After step III purification (Anion exchange with 4N HCl washed)

Hot cell with robots

Hot cell

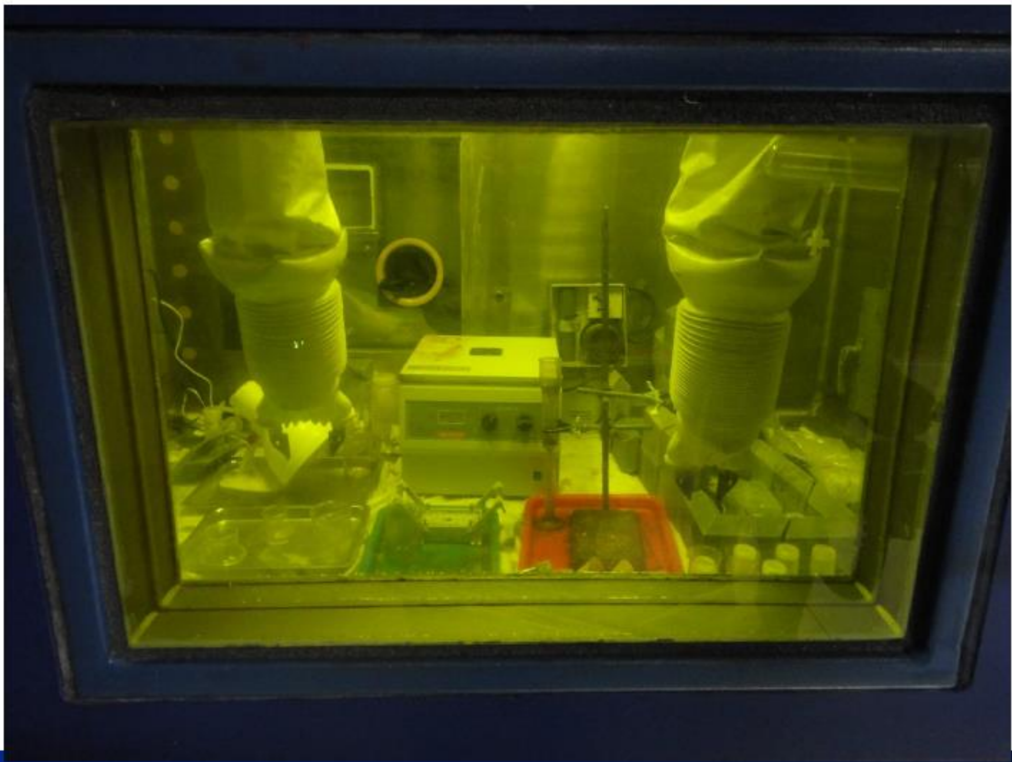

Solid target and adsorbent glass column

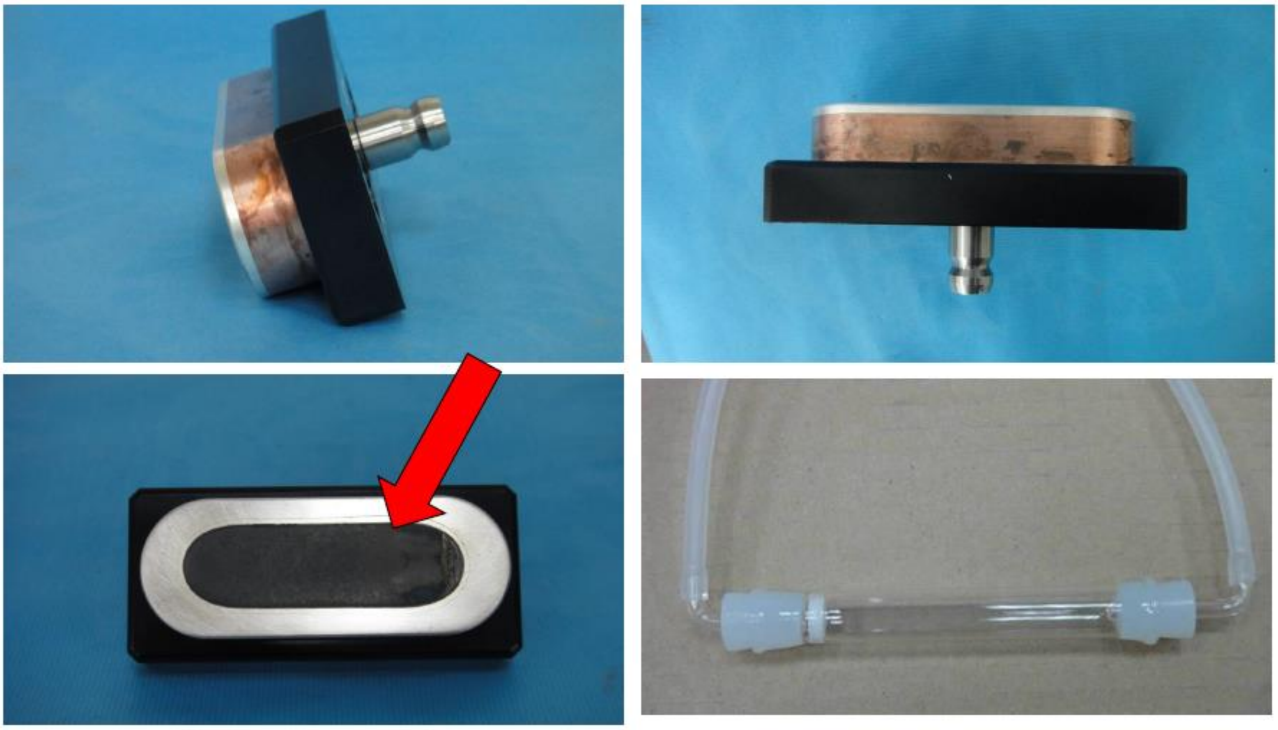

Ga-68 generator configuration

Outline

- **Ga-68/Ge-68 Generator**
- **Our systematic innovation ：**
  - Irradiation Product with Minimal Impurity
  - Method of Purification for Recycling of Ga-69 Isotope
  - The dual-core Ga-68 Radionuclide Generator
  - Automatic Synthesizer Apparatus for Producing Ga-68-DOTATATE
- **New drug application**

Method Used to Yield Irradiation Product with Minimal Impurity for Solid Target for Ga-68/Ge-68 Generator

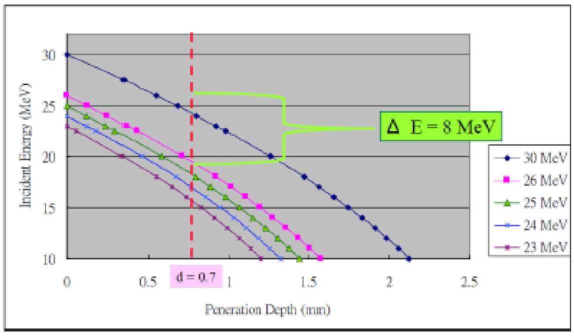

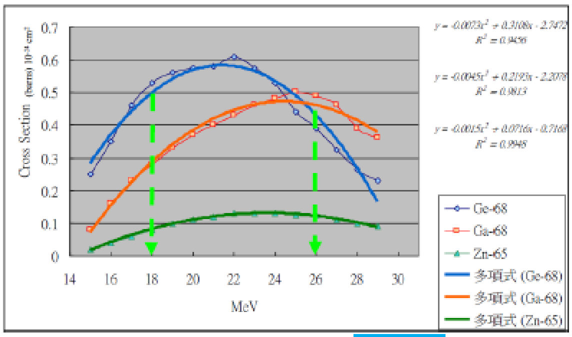

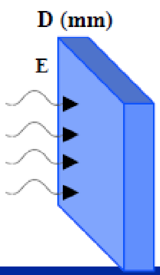

◎ Ga-68核種之反應式

$^{69}Ga(p,2n) \rightarrow {}^{68}Ge$

$^{68}Ge \xrightarrow[275\ d]{\varepsilon} {}^{68}Ga \xrightarrow[68\ min]{\varepsilon,\gamma,\beta} {}^{68}Zn$

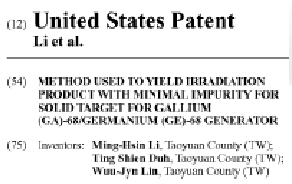
(12) United States Patent
Li et al.

(54) METHOD USED TO YIELD IRRADIATION PRODUCT WITH MINIMAL IMPURITY FOR SOLID TARGET FOR GALLIUM (GA)-68/GERMANIUM (GE)-68 GENERATOR

(75) Inventors: Ming-Hsin Li, Taoyuan County (TW); Ting Shien Duh, Taoyuan County (TW); Wuu-Jyh Lin, Taoyuan County (TW)

US 8239159, 2012

2014

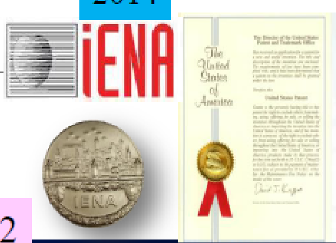

Method of Purification for Recycling of Ga-69 Isotope

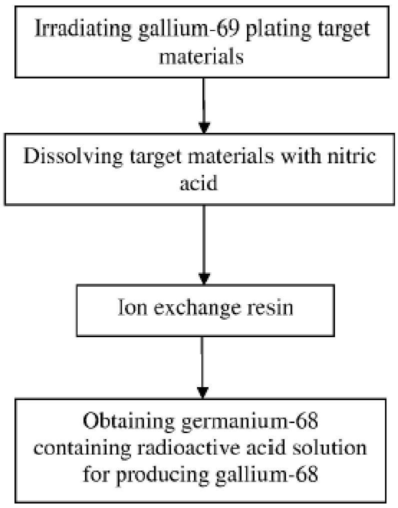

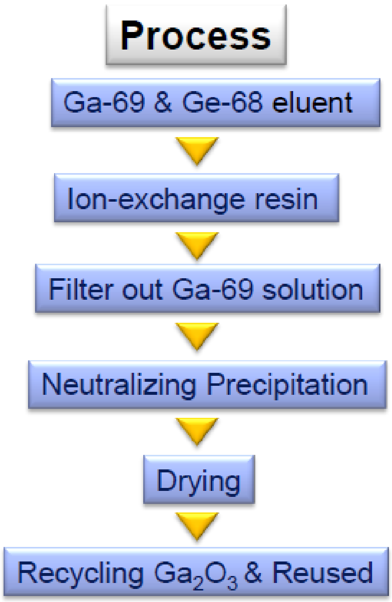

United States Patent
Li et al.

METHOD OF PURIFICATION FOR RECYCLING OF GALLIUM-69 ISOTOPE

Inventors: Ming-Hsin Li, Taoyuan County (TW); Hsin-Han Hsieh, Taoyuan County (TW)

US8894860 B2, 2014

The dual-core Ga-68 Radionuclide Generator Structure

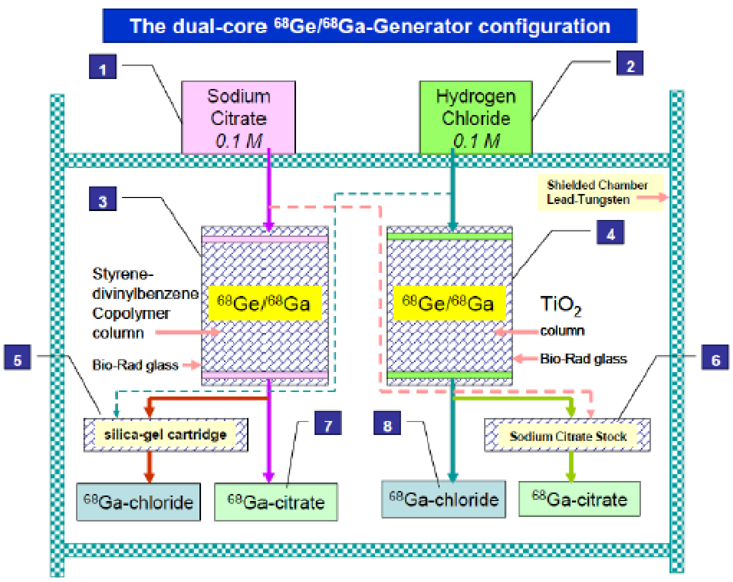

US8802014 B2, 2014

United States Patent
Li et al.

GA-68 RADIONUCLIDE GENERATOR STRUCTURE

Inventors: Ming-Hsin Li, Taoyuan County (TW); Jin-Jenn Lin, Taoyuan County (TW); Ther-Jen Ting, Taoyuan County (TW); I-Lea Dai, Taoyuan County (TW)

Automatic Synthesizer Apparatus for Producing Ga-68-DOTATATE and Method Thereof

US9266084 B2, 2016

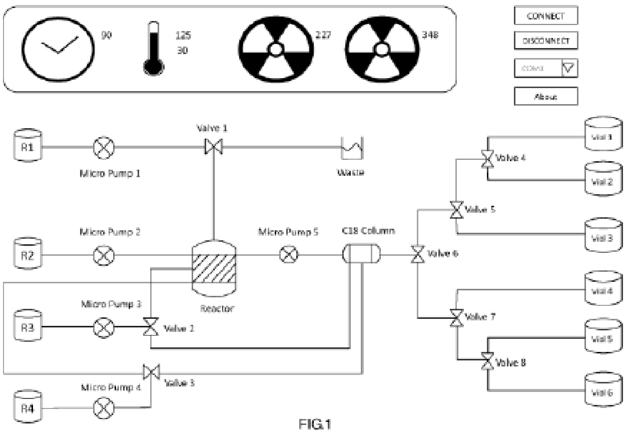

FIG.1

United States Patent
Li et al.

AUTOMATIC SYNTHESIZER APPARATUS FOR PRODUCING RADIOPHARMACEUTICAL TUMOR IMAGING AGENT GALLIUM-68-DOTATATE AND METHOD THEREOF

Applicants: **Ming-Hsin Li**, Taoyuan County (TW); **Hsin-Han Hsieh**, Taoyuan County (TW)

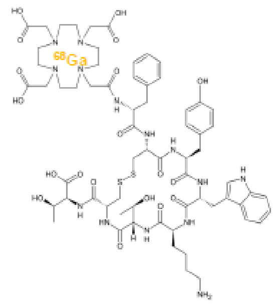

Ga-68-DOTATATE

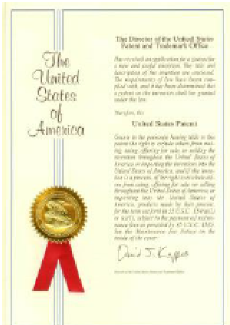

Outline

- Ga-68/Ge-68 Generator
- Our systematic innovation ：
  - Irradiation Product with Minimal Impurity
  - Method of Purification for Recycling of Ga-69 Isotope
  - The dual-core Ga-68 Radionuclide Generator
  - Automatic Synthesizer Apparatus for Producing Ga-68-DOTATATE
- **New drug application**

Principle of Ga-68 Positron Emission Tomography (PET)

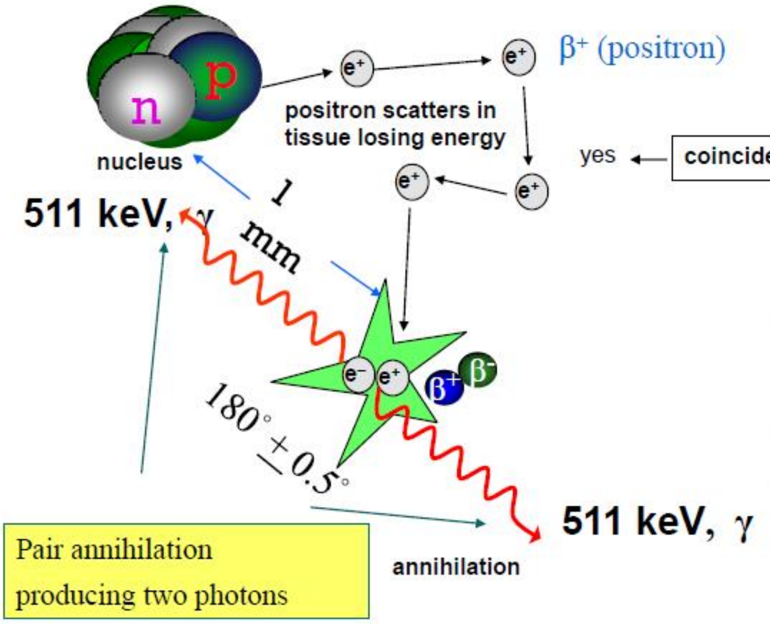

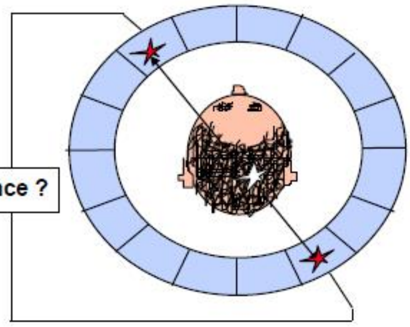

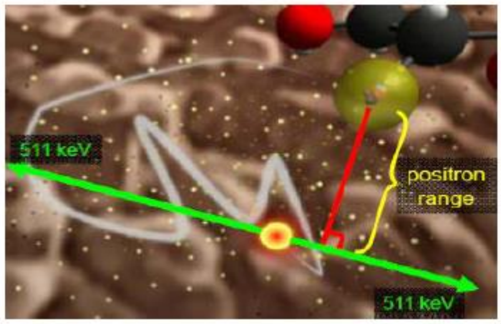

Ga-68 DOTATOC PET vs.SPECT and CT

Comparison of 3 Imaging Modalities: PET, SPECT, and CT

Parameter	PET (%)	SPECT (%)	CT (%)
Sensitivity	97 (69/71)	52 (37/71)	61 (41/67)
Specificity	92 (12/13)	92 (12/13)	71 (12/17)
Accuracy	96 (81/84)	58 (49/84)	63 (53/84)

The added value in diagnostic accuracy has an important influence on patient management

THE JOURNAL OF NUCLEAR MEDICINE • Vol. 48 • No. 4 • April 2007

DOTA-somatostatin analogue

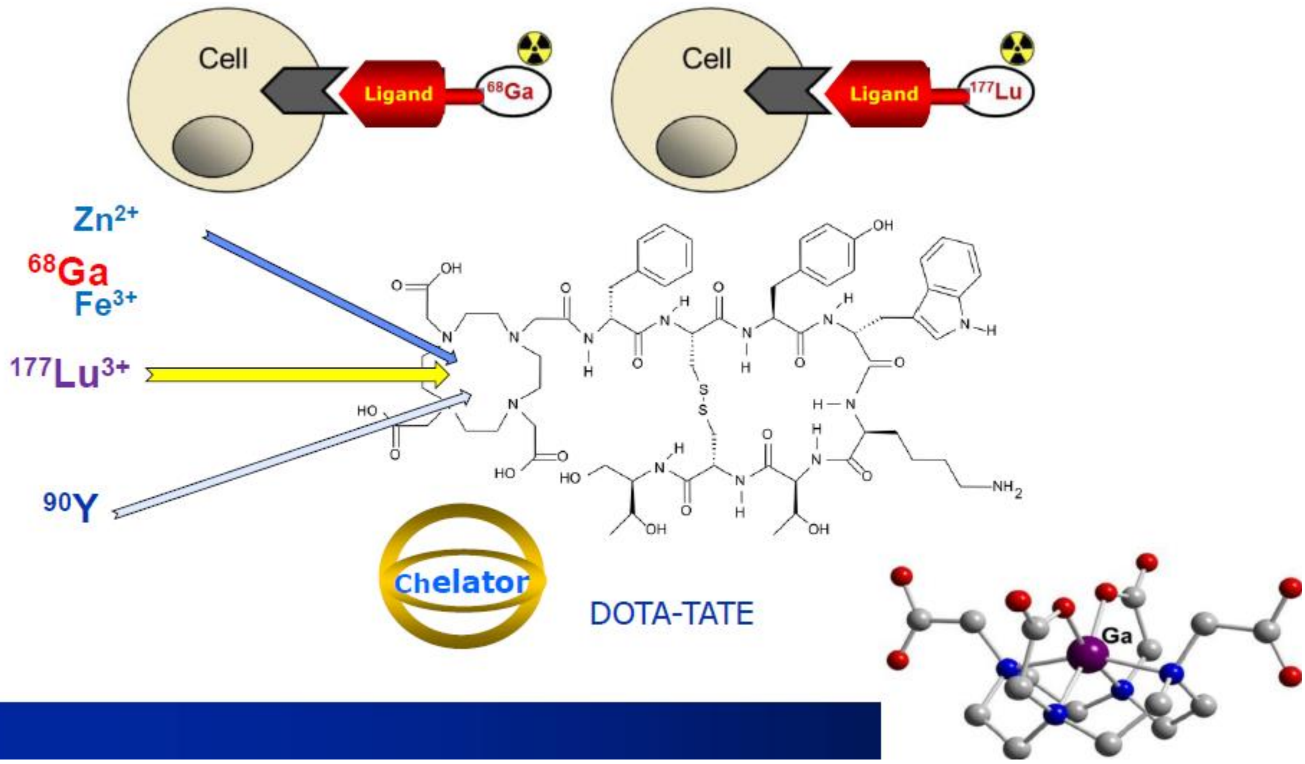

Pancreatic body and tail cancer

Ga-68-DOTA-TATE imaging

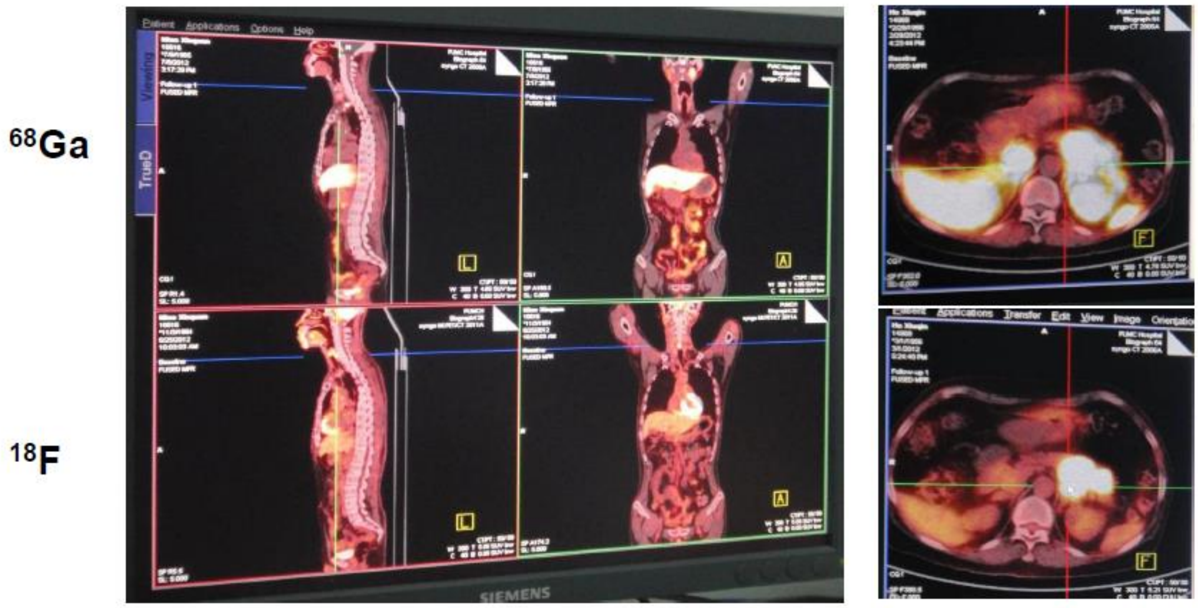

New drug Nano-PET/CT imaging at INER

^{68}Ga-DOTA-PEG$_2$-SP90 in 4T1 solid tumor

Animal model :
4T1 breast tumor-bearing mice

No.2

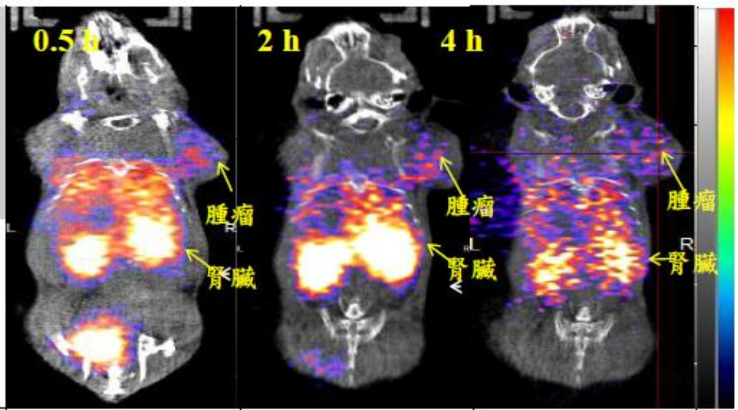

Bio-distribution (%ID/g)	Tumor	6.89	6.48	3.67
	Kidney	38.58	15.40	11.90
	Liver	6.15	6.58	3.81
	Muscle	3.80	4.90	2.34
T/M ratio		1.81	1.32	1.57
T/Liver ratio		1.12	0.99	0.96
T/Kidney ratio		0.18	0.42	0.31

New drug Nano-PET/CT imaging at INER

Ga-68-DOTA-PEG2-SP90-BT-483-2h

Targeted drug delivery systems mediated by a novel Peptide in breast cancer therapy and imaging

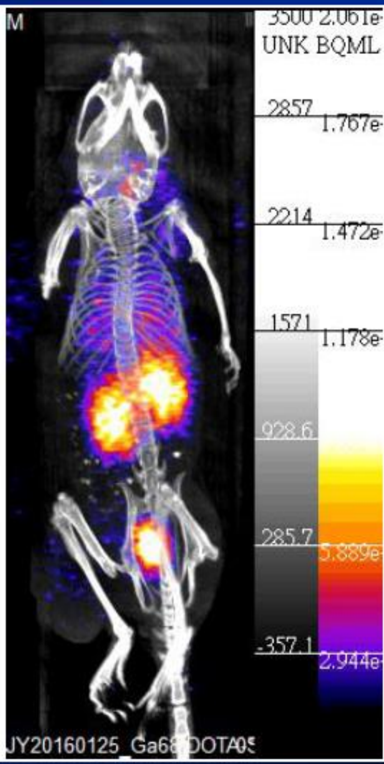

Conclusion

- ^{68}Ga is a promising PET isotope
- Independant from cyclotron
- 50mCi Generator are available
- Use is established in PET centers

But:

- Not yet registered as radiopharmaceutical
- Logistics must be improved

附件八：PBNC 2016 壁報論文展示內容

XI'AN JIAOTONG UNIVERSITY

Propagation of Nuclear-data Uncertainties for PWR Burnup Calculation

Chenghui Wan[1], *Liangzhi Cao*[1], *Hongchun Wu*[1], *Tiejun Zu*[1], *Wei Shen*[1,2]

1 *School of Nuclear Science and Technology, Xi'an Jiaotong University, Xi'an, Shaanxi, China, 710049*

2 *Canadian Nuclear Safety Commission, Ottawa, Ontario, Canada*

1.Introduction

- **Uncertainty Analysis for Neutronics Calculations**

Recently, the imprecision of cross sections, which would introduce uncertainties to responses of neutronics calculations, has been treated as one of the most significant sources of uncertainty. Uncertainty analysis (UA) is a proper way to determine the appropriate design margins.

- **Uncertainty Analysis for Burnup Calculation**

The burnup calculation is the coupling simulation of the neutron-transport and depletion calculations. Theoretical difficulties exist for the deterministic method (PT) as the coupled calculations and multi responses. While for the statistical sampling method, the coupled calculations can be considered conveniently, and no limit to the responses.

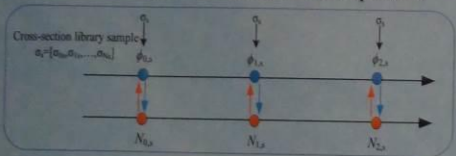

Fig.1 UA for burnup calculation using statistical sampling method

2.Calculation model

- **Overview of the UNICORN code**

Generating the samples of cross-section library is actually the process of perturbing the library around the expectation values, according to the cross-section covariance matrices.

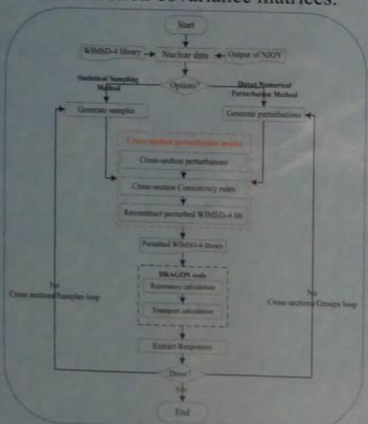

Fig.2 Flowchart of the UNICORN code

- **Perturbation propagations**

For the cross sections without resonance:

$$\sigma'_{x,g}(T)=\frac{\int_{\Delta E_g}\sigma'_x(E,T)\phi(E)dE}{\int_{\Delta E_g}\phi(E)dE}=(1+\delta_{x,g})\sigma_{x,g}(T)$$

For the cross sections with resonances:

$$\sigma'_{x,g}(T,\sigma_0)=\frac{\int_{\Delta E_g}\sigma'_x(E,T)\phi(E,\sigma_0)dE}{\int_{\Delta E_g}\phi(E,\sigma_0)dE}=(1+\delta_{x,g})\sigma_{x,g}(T,\sigma_0)\quad \sigma'_0=\frac{\sigma_0}{1+\delta_{t,g}}$$

3.Results

Relative uncertainties of k_{inf}, few-group cross sections and atomic densities with the depletions have been quantified applying the UNICORN code. The comparisons of relative uncertainty (%) for the atomic densities between UNICORN and TMC approach are as shown in Table 1.

Table 1. Result comparisons between UNICORN and the TMC approach

Iso.	10.0Gwd/tU		30.0Gwd/tU		50.0Gwd/tU		60.0Gwd/tU	
	1	2	1	2	1	2	1	2
^{134}Cs	4.71	5.23	4.38	4.94	4.06	4.56	3.89	4.35
^{143}Nd	0.29	0.31	0.91	0.96	1.60	1.73	1.97	2.16
^{149}Sm	5.07	5.06	5.24	5.23	5.46	5.55	5.58	5.75
^{151}Sm	5.50	4.87	6.64	5.99	6.90	6.35	6.98	6.50
^{151}Eu	4.85	4.33	6.63	6.18	7.06	6.98	7.26	7.43
^{155}Eu	27.9	26.3	33.2	31.1	35.4	32.9	35.6	33.1
^{155}Gd	27.3	25.3	29.9	27.9	28.3	26.4	26.7	25.0
^{234}U	0.31	0.32	0.98	1.05	1.74	1.92	2.15	2.40
^{235}U	0.11	0.11	0.48	0.54	1.22	1.49	1.78	2.24
^{236}U	1.50	1.41	1.44	1.39	1.40	1.42	1.39	1.48
^{237}Np	4.10	4.00	3.34	3.82	3.11	3.59	3.03	3.46
^{238}Pu	4.60	4.10	3.41	3.73	3.01	3.40	2.89	3.26
^{239}Pu	1.15	1.54	1.43	1.93	1.81	2.44	2.00	2.69
^{240}Pu	1.57	1.84	1.78	2.13	2.01	2.46	2.12	2.63
^{241}Pu	1.49	1.88	1.43	1.77	1.72	2.11	1.91	2.35
^{242}Pu	2.72	2.95	2.46	2.64	2.41	2.54	2.43	2.51
^{243}Am	2.95	3.21	2.59	2.89	2.36	2.74	2.26	2.68
^{244}Cm	3.21	3.49	2.92	3.21	2.73	3.11	2.67	3.10

- 1 represents the relative uncertainties obtained and published by the TMC approach
- 2 stands for the relative uncertainties obtained by UNICORN

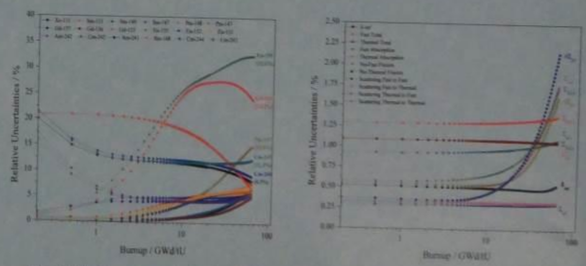

Fig.3 Relative uncertainties for TMI-1 pin-cell burnup calculation with UNICORN

4.Summary

UA has been performed to TMI-1 pin-cell burnup calculation, and it can be observed that:

- $\Delta k_{inf}/k_{inf}$ ~ 0.53% at BOC and 0.54% at EOC;
- $\Delta \nu\Sigma_{f,2}/\nu\Sigma_{f,2}$ ~ 0.84% at BOC and 2.15% at EOC;
- $\Delta\Sigma_{t,2}/\Sigma_{t,2}$ ~ 0.30% at BOC and 0.31% at EOC;
- At EOC:

$\Delta N(^{155}Eu)/N(^{155}Eu)$ ~ 32.6%, $\Delta N(^{155}Gd)/N(^{155}Gd)$ ~ 24.2%,
$\Delta N(^{147}Pm)/N(^{147}Pm)$ ~ 15.0%, $\Delta N(^{243}Cm)/N(^{243}Cm)$ ~ 12.4%,
$\Delta N(^{244}Cm)/N(^{244}Cm)$ ~ 8.3%.

Chenghui Wan, PH.D candidate
Nuclear Engineering Computational Physics (NECP)
School of Nuclear Science and Technology,Xi'an Jiaotong University
Email: chenghuiwan@stu.xjtu.edu.cn

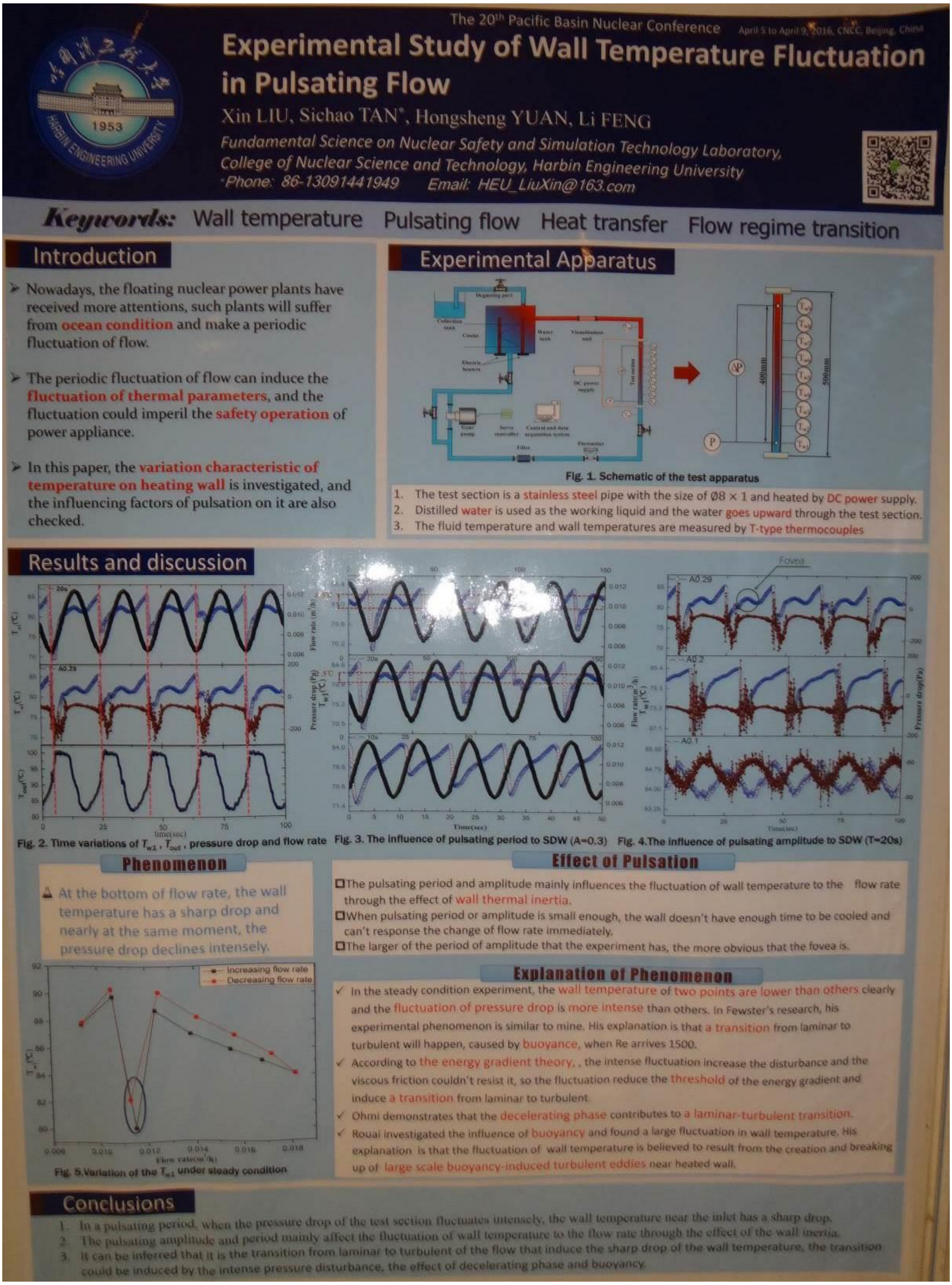

The 20th Pacific Basin Nuclear Conference
April 5 to April 9, 2016, CNCC, Beijing, China
Experimental Study of Wall Temperature Fluctuation in Pulsating Flow
Xin LIU, Sichao TAN*, Hongsheng YUAN, Li FENG
Fundamental Science on Nuclear Safety and Simulation Technology Laboratory,
College of Nuclear Science and Technology, Harbin Engineering University
*Phone: 86-13091441949 Email: HEU_LiuXin@163.com
Keywords: Wall temperature Pulsating flow Heat transfer Flow regime transition
Introduction
Nowadays, the floating nuclear power plants have received more attentions, such plants will suffer from ocean condition and make a periodic fluctuation of flow.
The periodic fluctuation of flow can induce the fluctuation of thermal parameters, and the fluctuation could imperil the safety operation of power appliance.
In this paper, the variation characteristic of temperature on heating wall is investigated, and the influencing factors of pulsation on it are also checked.
Experimental Apparatus
Fig. 1. Schematic of the test apparatus
1. The test section is a stainless steel pipe with the size of Ø8 × 1 and heated by DC power supply.
2. Distilled water is used as the working liquid and the water goes upward through the test section.
3. The fluid temperature and wall temperatures are measured by T-type thermocouples
Results and discussion
Fig. 2. Time variations of Tw1, Tout, pressure drop and flow rate
Fig. 3. The influence of pulsating period to SDW (A=0.3)
Fig. 4. The influence of pulsating amplitude to SDW (T=20s)
Phenomenon
At the bottom of flow rate, the wall temperature has a sharp drop and nearly at the same moment, the pressure drop declines intensely.
Increasing flow rate
Decreasing flow rate
Fig. 5. Variation of the Tw1 under steady condition
Effect of Pulsation
The pulsating period and amplitude mainly influences the fluctuation of wall temperature to the flow rate through the effect of wall thermal inertia.
When pulsating period or amplitude is small enough, the wall doesn't have enough time to be cooled and can't response the change of flow rate immediately.
The larger of the period of amplitude that the experiment has, the more obvious that the fovea is.
Explanation of Phenomenon
In the steady condition experiment, the wall temperature of two points are lower than others clearly and the fluctuation of pressure drop is more intense than others. In Fewster's research, his experimental phenomenon is similar to mine. His explanation is that a transition from laminar to turbulent will happen, caused by buoyance, when Re arrives 1500.
According to the energy gradient theory, , the intense fluctuation increase the disturbance and the viscous friction couldn't resist it, so the fluctuation reduce the threshold of the energy gradient and induce a transition from laminar to turbulent.
Ohmi demonstrates that the decelerating phase contributes to a laminar-turbulent transition.
Rouai investigated the influence of buoyancy and found a large fluctuation in wall temperature. His explanation is that the fluctuation of wall temperature is believed to result from the creation and breaking up of large scale buoyancy-induced turbulent eddies near heated wall.
Conclusions
1. In a pulsating period, when the pressure drop of the test section fluctuates intensely, the wall temperature near the inlet has a sharp drop.
2. The pulsating amplitude and period mainly affect the fluctuation of wall temperature to the flow rate through the effect of the wall inertia.
3. It can be inferred that it is the transition from laminar to turbulent of the flow that induce the sharp drop of the wall temperature, the transition could be induced by the intense pressure disturbance, the effect of decelerating phase and buoyancy.

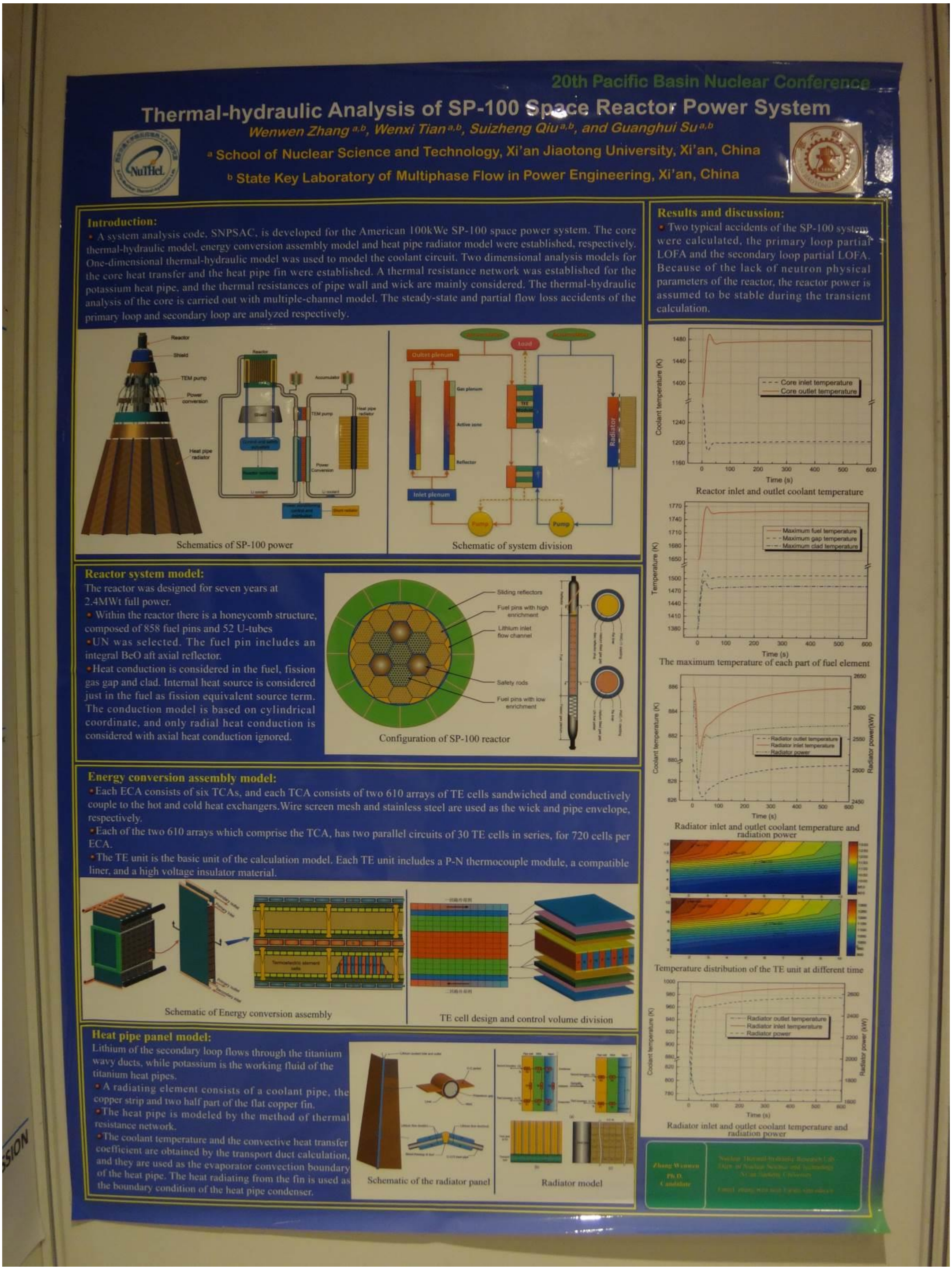
20th Pacific Basin Nuclear Conference
Thermal-hydraulic Analysis of SP-100 Space Reactor Power System
Wenwen Zhang a,b, Wenxi Tian a,b, Suizheng Qiu a,b, and Guanghui Su a,b
a School of Nuclear Science and Technology, Xi'an Jiaotong University, Xi'an, China
b State Key Laboratory of Multiphase Flow in Power Engineering, Xi'an, China
Introduction:
A system analysis code, SNPSAC, is developed for the American 100kWe SP-100 space power system. The core thermal-hydraulic model, energy conversion assembly model and heat pipe radiator model were established, respectively. One-dimensional thermal-hydraulic model was used to model the coolant circuit. Two dimensional analysis models for the core heat transfer and the heat pipe fin were established. A thermal resistance network was established for the potassium heat pipe, and the thermal resistances of pipe wall and wick are mainly considered. The thermal-hydraulic analysis of the core is carried out with multiple-channel model. The steady-state and partial flow loss accidents of the primary loop and secondary loop are analyzed respectively.
Schematics of SP-100 power
Schematic of system division
Reactor system model:
The reactor was designed for seven years at 2.4MWt full power.
Within the reactor there is a honeycomb structure, composed of 858 fuel pins and 52 U-tubes
UN was selected. The fuel pin includes an integral BeO aft axial reflector.
Heat conduction is considered in the fuel, fission gas gap and clad. Internal heat source is considered just in the fuel as fission equivalent source term. The conduction model is based on cylindrical coordinate, and only radial heat conduction is considered with axial heat conduction ignored.
Configuration of SP-100 reactor
Energy conversion assembly model:
Each ECA consists of six TCAs, and each TCA consists of two 610 arrays of TE cells sandwiched and conductively couple to the hot and cold heat exchangers. Wire screen mesh and stainless steel are used as the wick and pipe envelope, respectively.
Each of the two 610 arrays which comprise the TCA, has two parallel circuits of 30 TE cells in series, for 720 cells per ECA.
The TE unit is the basic unit of the calculation model. Each TE unit includes a P-N thermocouple module, a compatible liner, and a high voltage insulator material.
Schematic of Energy conversion assembly
TE cell design and control volume division
Heat pipe panel model:
Lithium of the secondary loop flows through the titanium wavy ducts, while potassium is the working fluid of the titanium heat pipes.
A radiating element consists of a coolant pipe, the copper strip and two half part of the flat copper fin.
The heat pipe is modeled by the method of thermal resistance network.
The coolant temperature and the convective heat transfer coefficient are obtained by the transport duct calculation, and they are used as the evaporator convection boundary of the heat pipe. The heat radiating from the fin is used as the boundary condition of the heat pipe condenser.
Schematic of the radiator panel
Radiator model
Results and discussion:
Two typical accidents of the SP-100 system were calculated, the primary loop partial LOFA and the secondary loop partial LOFA. Because of the lack of neutron physical parameters of the reactor, the reactor power is assumed to be stable during the transient calculation.
Reactor inlet and outlet coolant temperature
The maximum temperature of each part of fuel element
Radiator inlet and outlet coolant temperature and radiation power
Temperature distribution of the TE unit at different time
Radiator inlet and outlet coolant temperature and radiation power

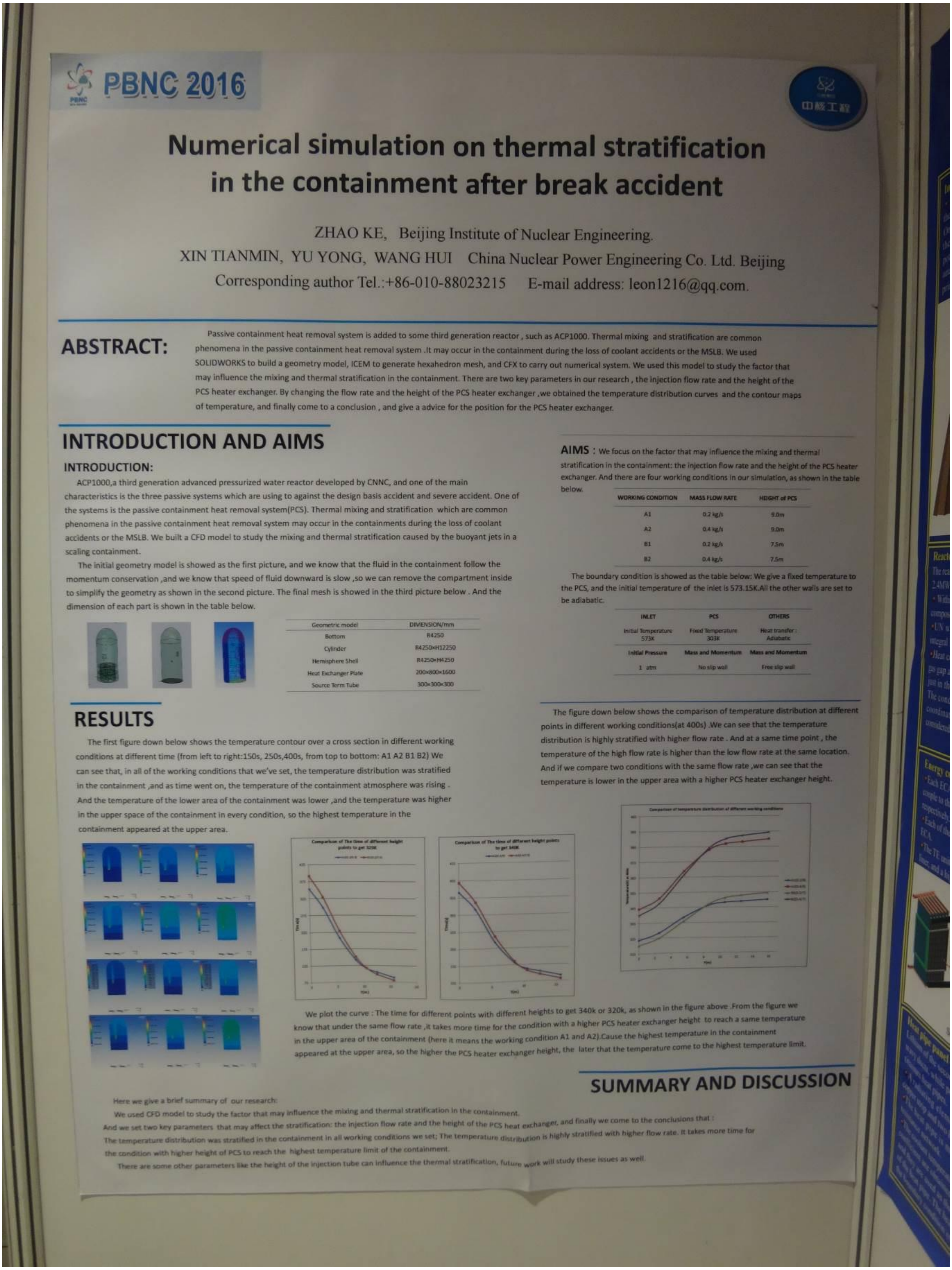

PBNC 2016

中核工程

Numerical simulation on thermal stratification in the containment after break accident

ZHAO KE, Beijing Institute of Nuclear Engineering.

XIN TIANMIN, YU YONG, WANG HUI China Nuclear Power Engineering Co. Ltd. Beijing

Corresponding author Tel.:+86-010-88023215 E-mail address: leon1216@qq.com.

ABSTRACT:

Passive containment heat removal system is added to some third generation reactor , such as ACP1000. Thermal mixing and stratification are common phenomena in the passive containment heat removal system .It may occur in the containment during the loss of coolant accidents or the MSLB. We used SOLIDWORKS to build a geometry model, ICEM to generate hexahedron mesh, and CFX to carry out numerical system. We used this model to study the factor that may influence the mixing and thermal stratification in the containment. There are two key parameters in our research , the injection flow rate and the height of the PCS heater exchanger. By changing the flow rate and the height of the PCS heater exchanger ,we obtained the temperature distribution curves and the contour maps of temperature, and finally come to a conclusion , and give a advice for the position for the PCS heater exchanger.

INTRODUCTION AND AIMS

INTRODUCTION:

ACP1000,a third generation advanced pressurized water reactor developed by CNNC, and one of the main characteristics is the three passive systems which are using to against the design basis accident and severe accident. One of the systems is the passive containment heat removal system(PCS). Thermal mixing and stratification which are common phenomena in the passive containment heat removal system may occur in the containments during the loss of coolant accidents or the MSLB. We built a CFD model to study the mixing and thermal stratification caused by the buoyant jets in a scaling containment.

The initial geometry model is showed as the first picture, and we know that the fluid in the containment follow the momentum conservation ,and we know that speed of fluid downward is slow ,so we can remove the compartment inside to simplify the geometry as shown in the second picture. The final mesh is showed in the third picture below . And the dimension of each part is shown in the table below.

Geometric model	DIMENSION/mm
Bottom	R4250
Cylinder	R4250×H12250
Hemisphere Shell	R4250×H4250
Heat Exchanger Plate	200×800×1600
Source Term Tube	300×300×300

AIMS : We focus on the factor that may influence the mixing and thermal stratification in the containment: the injection flow rate and the height of the PCS heater exchanger. And there are four working conditions in our simulation, as shown in the table below.

WORKING CONDITION	MASS FLOW RATE	HEIGHT of PCS
A1	0.2 kg/s	9.0m
A2	0.4 kg/s	9.0m
B1	0.2 kg/s	7.5m
B2	0.4 kg/s	7.5m

The boundary condition is showed as the table below: We give a fixed temperature to the PCS, and the initial temperature of the inlet is 573.15K.All the other walls are set to be adiabatic.

INLET	PCS	OTHERS
Initial Temperature 573K	Fixed Temperature 303K	Heat transfer : Adiabatic
Initial Pressure	Mass and Momentum	Mass and Momentum
1 atm	No slip wall	Free slip wall

RESULTS

The first figure down below shows the temperature contour over a cross section in different working conditions at different time (from left to right:150s, 250s,400s, from top to bottom: A1 A2 B1 B2) We can see that, in all of the working conditions that we've set, the temperature distribution was stratified in the containment ,and as time went on, the temperature of the containment atmosphere was rising . And the temperature of the lower area of the containment was lower ,and the temperature was higher in the upper space of the containment in every condition, so the highest temperature in the containment appeared at the upper area.

The figure down below shows the comparison of temperature distribution at different points in different working conditions(at 400s) .We can see that the temperature distribution is highly stratified with higher flow rate . And at a same time point , the temperature of the high flow rate is higher than the low flow rate at the same location. And if we compare two conditions with the same flow rate ,we can see that the temperature is lower in the upper area with a higher PCS heater exchanger height.

We plot the curve : The time for different points with different heights to get 340k or 320k, as shown in the figure above .From the figure we know that under the same flow rate ,it takes more time for the condition with a higher PCS heater exchanger height to reach a same temperature in the upper area of the containment (here it means the working condition A1 and A2).Cause the highest temperature in the containment appeared at the upper area, so the higher the PCS heater exchanger height, the later that the temperature come to the highest temperature limit.

SUMMARY AND DISCUSSION

Here we give a brief summary of our research:

We used CFD model to study the factor that may influence the mixing and thermal stratification in the containment.

And we set two key parameters that may affect the stratification: the injection flow rate and the height of the PCS heat exchanger, and finally we come to the conclusions that :

The temperature distribution was stratified in the containment in all working conditions we set; The temperature distribution is highly stratified with higher flow rate. It takes more time for the condition with higher height of PCS to reach the highest temperature limit of the containment.

There are some other parameters like the height of the injection tube can influence the thermal stratification, future work will study these issues as well.

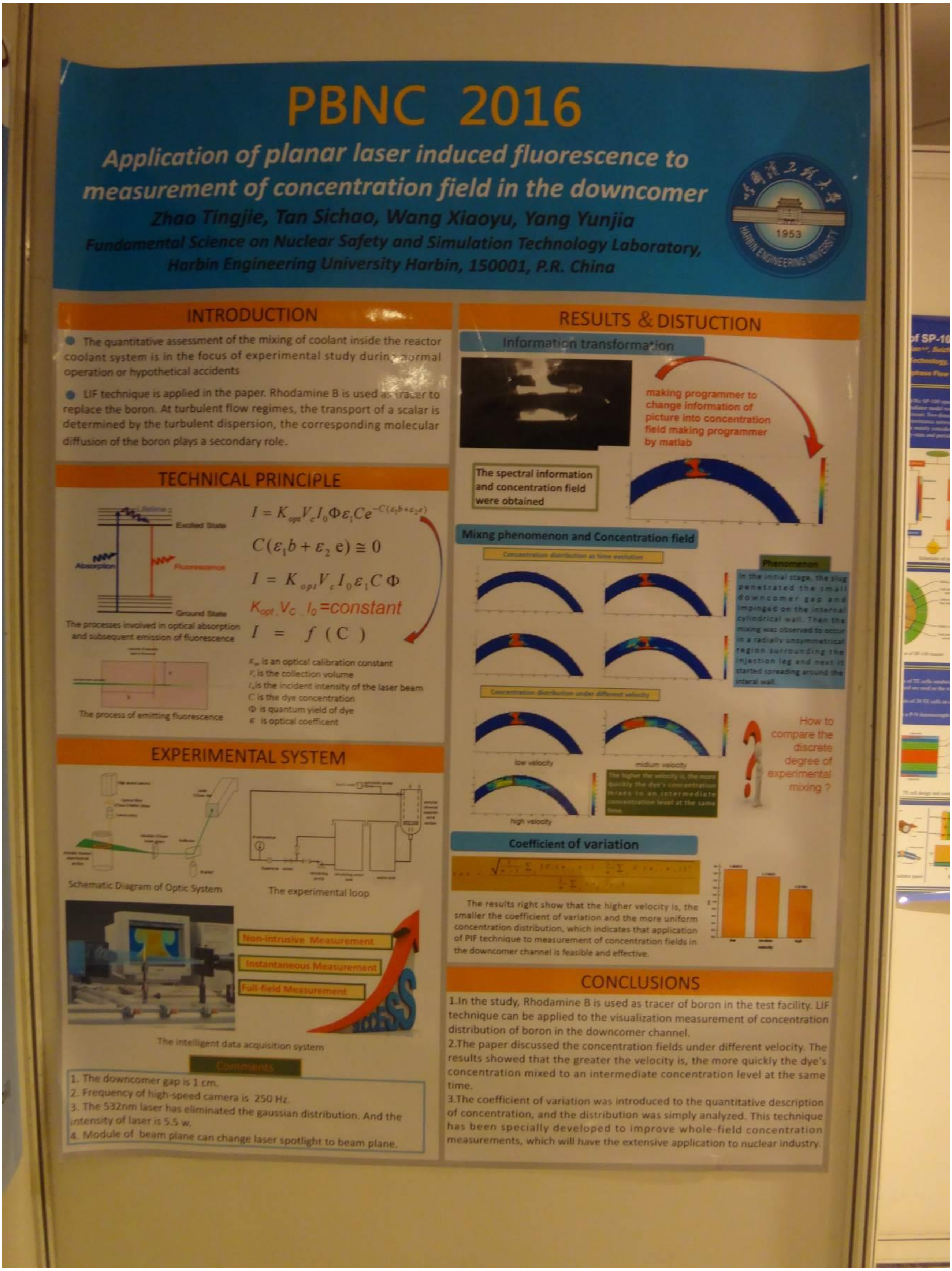
PBNC 2016
Application of planar laser induced fluorescence to measurement of concentration field in the downcomer
Zhao Tingjie, Tan Sichao, Wang Xiaoyu, Yang Yunjia
Fundamental Science on Nuclear Safety and Simulation Technology Laboratory, Harbin Engineering University Harbin, 150001, P.R. China
1953
HARBIN ENGINEERING UNIVERSITY
INTRODUCTION
The quantitative assessment of the mixing of coolant inside the reactor coolant system is in the focus of experimental study during normal operation or hypothetical accidents
LIF technique is applied in the paper. Rhodamine B is used as tracer to replace the boron. At turbulent flow regimes, the transport of a scalar is determined by the turbulent dispersion, the corresponding molecular diffusion of the boron plays a secondary role.
TECHNICAL PRINCIPLE
Excited State
Absorption
Fluorescence
Ground State
The processes involved in optical absorption and subsequent emission of fluorescence
The process of emitting fluorescence
$I = K_{opt} V_c I_0 \Phi \varepsilon_1 C e^{-C(\varepsilon_1 b + \varepsilon_2 e)}$
$C(\varepsilon_1 b + \varepsilon_2 e) \cong 0$
$I = K_{opt} V_c I_0 \varepsilon_1 C \Phi$
K_{opt}, V_C, I_0=constant
$I = f(C)$
K_{opt} is an optical calibration constant
V_c is the collection volume
I_0 is the incident intensity of the laser beam
C is the dye concentration
Φ is quantum yield of dye
ε is optical coefficent
EXPERIMENTAL SYSTEM
Schematic Diagram of Optic System
The experimental loop
Non-intrusive Measurement
Instantaneous Measurement
Full-field Measurement
The intelligent data acquisition system
Comments
1. The downcomer gap is 1 cm.
2. Frequency of high-speed camera is 250 Hz.
3. The 532nm laser has eliminated the gaussian distribution. And the intensity of laser is 5.5 w.
4. Module of beam plane can change laser spotlight to beam plane.
RESULTS & DISTUCTION
Information transformation
making programmer to change information of picture into concentration field making programmer by matlab
The spectral information and concentration field were obtained
Mixng phenomenon and Concentration field
Concentration distribution as time evolution
Phenomenon
In the initial stage, the slug penetrated the small downcomer gap and impinged on the internal cylindrical wall. Then the mixing was observed to occur in a radially unsymmetrical region surrounding the injection leg and next it started spreading around the interal wall.
Concentration distribution under different velocity
low velocity
midium velocity
high velocity
The higher the velocity is, the more quickly the dye's concentration mixes to an intermediate concentration level at the same time.
How to compare the discrete degree of experimental mixing ?
Coefficient of variation
The results right show that the higher velocity is, the smaller the coefficient of variation and the more uniform concentration distribution, which indicates that application of PIF technique to measurement of concentration fields in the downcomer channel is feasible and effective.
CONCLUSIONS
1.In the study, Rhodamine B is used as tracer of boron in the test facility. LIF technique can be applied to the visualization measurement of concentration distribution of boron in the downcomer channel.
2.The paper discussed the concentration fields under different velocity. The results showed that the greater the velocity is, the more quickly the dye's concentration mixed to an intermediate concentration level at the same time.
3.The coefficient of variation was introduced to the quantitative description of concentration, and the distribution was simply analyzed. This technique has been specially developed to improve whole-field concentration measurements, which will have the extensive application to nuclear industry.


Specific Activities of OBT in Soil around a Nuclear Power Plant
SINAP
Ke Deng (邓珂)
Shanghai Institute of Apply Physics
Chinese Academy of Science
OBT- Tritium atoms bound to organic molecules in biological samples
OBT
E-OBT
NE-OBT
Easily removed
Longer half-life
Higher effective dose coefficient
Experimental
1. Frozen dried
2. Immersed in tritium free rinse water
3. sieve shaker
4. Combustion, 8h, 850°C
5. Liquid scintillation counting
Results and conclusion
Soil surface
• OBT concentrated in the soil with particle size of 53-250μm
• OBT concentrate at sub-surface
• The closer to the source (NPP), the higher the concentration of OBT
Future work
• Investigate the distribution of microorganisms in soil (Depth, particle size of soil)
• Measure more samples from various source of OBT
• Investigate the formation and transportation of OBT in air

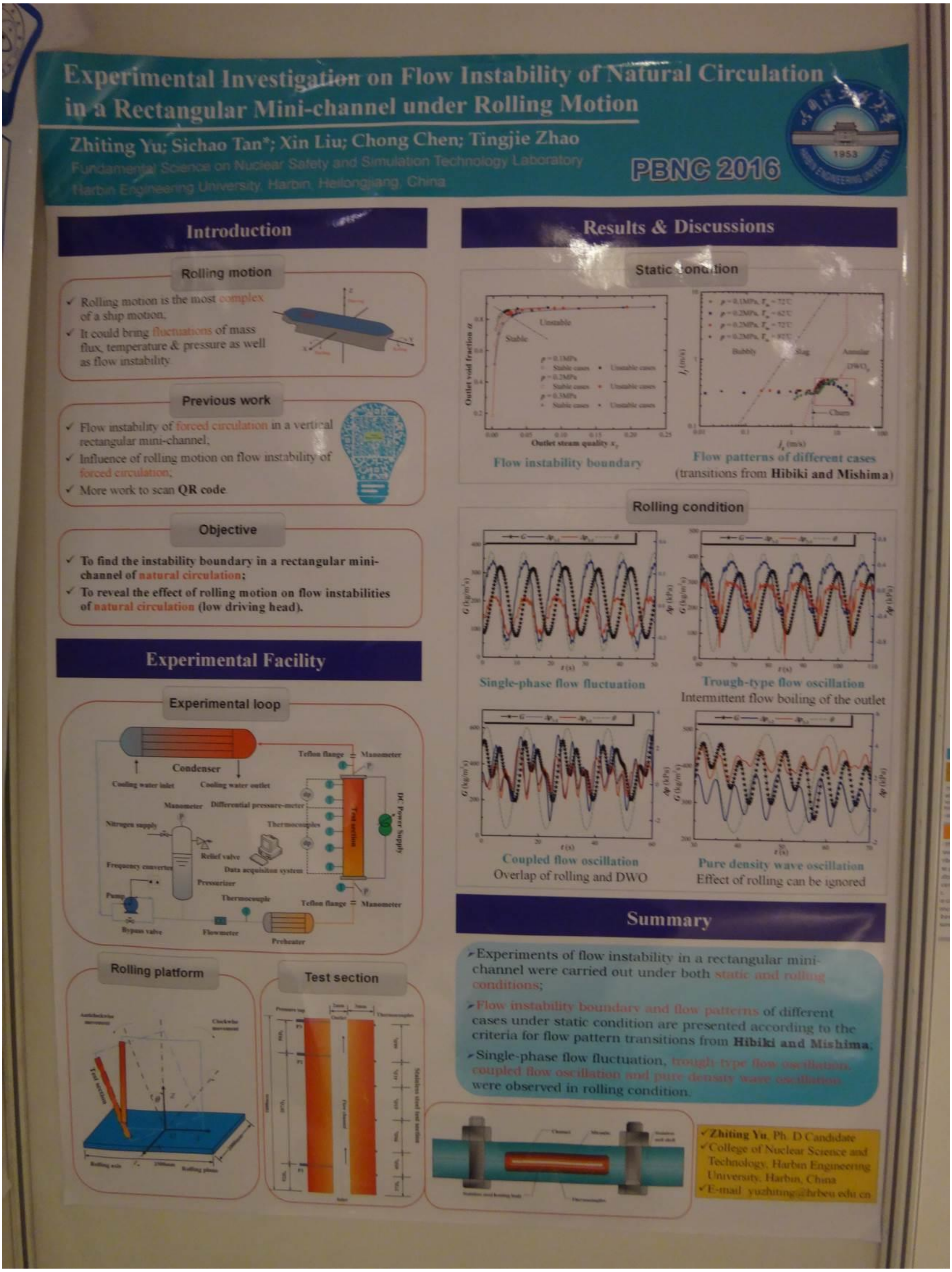
Experimental Investigation on Flow Instability of Natural Circulation in a Rectangular Mini-channel under Rolling Motion
Zhiting Yu; Sichao Tan*; Xin Liu; Chong Chen; Tingjie Zhao
Fundamental Science on Nuclear Safety and Simulation Technology Laboratory
Harbin Engineering University, Harbin, Heilongjiang, China
PBNC 2016
1953
Introduction
Rolling motion
Rolling motion is the most complex of a ship motion;
It could bring fluctuations of mass flux, temperature & pressure as well as flow instability
Previous work
Flow instability of forced circulation in a vertical rectangular mini-channel;
Influence of rolling motion on flow instability of forced circulation;
More work to scan QR code.
Objective
To find the instability boundary in a rectangular mini-channel of natural circulation;
To reveal the effect of rolling motion on flow instabilities of natural circulation (low driving head).
Experimental Facility
Experimental loop
Condenser
Cooling water inlet
Cooling water outlet
Teflon flange
Manometer
Differential pressure-meter
Nitrogen supply
Thermocouples
Test section
DC Power Supply
Relief valve
Data acquisition system
Frequency converter
Pressurizer
Pump
Thermocouple
Bypass valve
Flowmeter
Preheater
Rolling platform
Test section
Results & Discussions
Static condition
Outlet void fraction α
Outlet steam quality x_e
Unstable
Stable
Flow instability boundary
Bubbly
Slug
Annular
Churn
Flow patterns of different cases
(transitions from Hibiki and Mishima)
Rolling condition
Single-phase flow fluctuation
Trough-type flow oscillation
Intermittent flow boiling of the outlet
Coupled flow oscillation
Overlap of rolling and DWO
Pure density wave oscillation
Effect of rolling can be ignored
Summary
Experiments of flow instability in a rectangular mini-channel were carried out under both static and rolling conditions;
Flow instability boundary and flow patterns of different cases under static condition are presented according to the criteria for flow pattern transitions from Hibiki and Mishima;
Single-phase flow fluctuation, trough-type flow oscillation, coupled flow oscillation and pure density wave oscillation were observed in rolling condition.
Zhiting Yu, Ph. D Candidate
College of Nuclear Science and Technology, Harbin Engineering University, Harbin, China
E-mail: yuzhiting@hrbeu.edu.cn

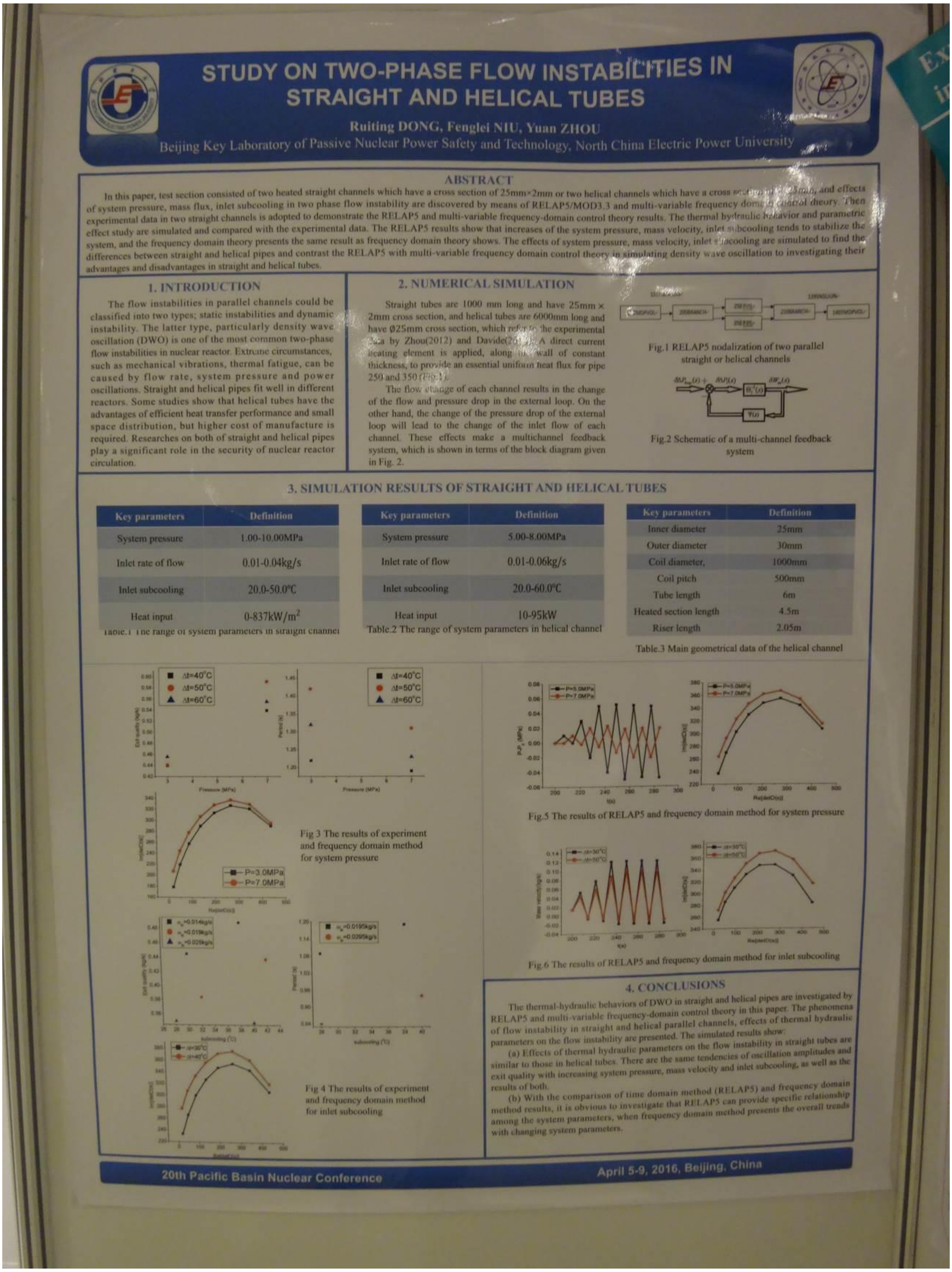

STUDY ON TWO-PHASE FLOW INSTABILITIES IN STRAIGHT AND HELICAL TUBES

Ruiting DONG, Fenglei NIU, Yuan ZHOU
Beijing Key Laboratory of Passive Nuclear Power Safety and Technology, North China Electric Power University

ABSTRACT

In this paper, test section consisted of two heated straight channels which have a cross section of 25mm×2mm or two helical channels which have a cross section of [illegible]mm, and effects of system pressure, mass flux, inlet subcooling in two phase flow instability are discovered by means of RELAP5/MOD3.3 and multi-variable frequency domain control theory. Then experimental data in two straight channels is adopted to demonstrate the RELAP5 and multi-variable frequency-domain control theory results. The thermal hydraulic behavior and parametric effect study are simulated and compared with the experimental data. The RELAP5 results show that increases of the system pressure, mass velocity, inlet subcooling tends to stabilize the system, and the frequency domain theory presents the same result as frequency domain theory shows. The effects of system pressure, mass velocity, inlet subcooling are simulated to find the differences between straight and helical pipes and contrast the RELAP5 with multi-variable frequency domain control theory in simulating density wave oscillation to investigating their advantages and disadvantages in straight and helical tubes.

1. INTRODUCTION

The flow instabilities in parallel channels could be classified into two types; static instabilities and dynamic instability. The latter type, particularly density wave oscillation (DWO) is one of the most common two-phase flow instabilities in nuclear reactor. Extreme circumstances, such as mechanical vibrations, thermal fatigue, can be caused by flow rate, system pressure and power oscillations. Straight and helical pipes fit well in different reactors. Some studies show that helical tubes have the advantages of efficient heat transfer performance and small space distribution, but higher cost of manufacture is required. Researches on both of straight and helical pipes play a significant role in the security of nuclear reactor circulation.

2. NUMERICAL SIMULATION

Straight tubes are 1000 mm long and have 25mm × 2mm cross section, and helical tubes are 6000mm long and have Ø25mm cross section, which refer to the experimental data by Zhou(2012) and Davide(20[illegible]). A direct current heating element is applied, along the wall of constant thickness, to provide an essential uniform heat flux for pipe 250 and 350 (Fig.1).

The flow change of each channel results in the change of the flow and pressure drop in the external loop. On the other hand, the change of the pressure drop of the external loop will lead to the change of the inlet flow of each channel. These effects make a multichannel feedback system, which is shown in terms of the block diagram given in Fig. 2.

Fig.1 RELAP5 nodalization of two parallel straight or helical channels

Fig.2 Schematic of a multi-channel feedback system

3. SIMULATION RESULTS OF STRAIGHT AND HELICAL TUBES

Key parameters	Definition
System pressure	1.00-10.00MPa
Inlet rate of flow	0.01-0.04kg/s
Inlet subcooling	20.0-50.0°C
Heat input	0-837kW/m^2

Table.1 The range of system parameters in straight channel

Key parameters	Definition
System pressure	5.00-8.00MPa
Inlet rate of flow	0.01-0.06kg/s
Inlet subcooling	20.0-60.0°C
Heat input	10-95kW

Table.2 The range of system parameters in helical channel

Key parameters	Definition
Inner diameter	25mm
Outer diameter	30mm
Coil diameter,	1000mm
Coil pitch	500mm
Tube length	6m
Heated section length	4.5m
Riser length	2.05m

Table.3 Main geometrical data of the helical channel

Fig 3 The results of experiment and frequency domain method for system pressure

Fig 4 The results of experiment and frequency domain method for inlet subcooling

Fig.5 The results of RELAP5 and frequency domain method for system pressure

Fig.6 The results of RELAP5 and frequency domain method for inlet subcooling

4. CONCLUSIONS

The thermal-hydraulic behaviors of DWO in straight and helical pipes are investigated by RELAP5 and multi-variable frequency-domain control theory in this paper. The phenomena of flow instability in straight and helical parallel channels, effects of thermal hydraulic parameters on the flow instability are presented. The simulated results show:

(a) Effects of thermal hydraulic parameters on the flow instability in straight tubes are similar to those in helical tubes. There are the same tendencies of oscillation amplitudes and exit quality with increasing system pressure, mass velocity and inlet subcooling, as well as the results of both.

(b) With the comparison of time domain method (RELAP5) and frequency domain method results, it is obvious to investigate that RELAP5 can provide specific relationship among the system parameters, when frequency domain method presents the overall trends with changing system parameters.

20th Pacific Basin Nuclear Conference

April 5-9, 2016, Beijing, China

Experimental Study on Natural Circulation flow in Rectangular Channel under Rolling

WANG Jiangwen, GAO Puzhen, CHEN Chong

Fundamental Science on Nuclear Safety and Simulation Technology Laboratory, Harbin Engineering University, China.

The 20th Pacific Basin Nuclear Conference, April 5 to April 9, 2016, CNCC, Beijing, China

ABSTRACT:

- The mechanical rolling thermal-hydraulic experimental facility is used to simulate the ship motion.
- The rolling motion can fluctuate the flow and the oscillating frequency of the flow is the same as the rolling frequency.
- For steady condition, Test and Allen methods can be used to predict the λ. The Gnielinski formula can't predict heat transfer coefficient for natural circulation. The result of new formula agrees with the experimental data.
- Rolling reduces the flow of natural circulation. And rolling enhances the heat transfer ability

INTRODUCTION:

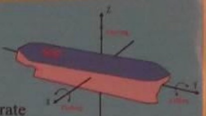

- Natural circulation is an important passive cooling mechanism. As no pumping power can be used, it is the only way to circulate fluids under accident.
- Affected by the ocean condition, the ship will generate rolling, heaving and pitching motions. And coolant flow is influenced by inertia force and inclination pipe.
- Rectangular channel is a good choice for compact heat exchanger.
- It is not very clear that the characteristics of natural circulation flow in rectangular channel under rolling motion condition.

EXPERIMENTAL APPARATUS

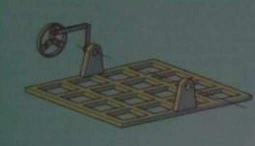

Crank and rocker mechanism and platform

Rolling angle:

$\theta_t = \theta_{max}\sin(2\pi t/T)$

Rolling amplitudes:

10°,15° and 20°

Rolling periods:

10s, 15s and 20s

Inlet temperature:

50℃ to 80℃

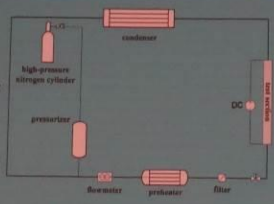

Experimental loop

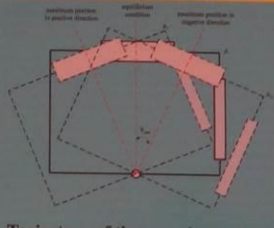

Trajectory of the experiment loop

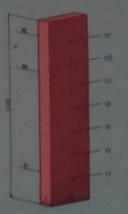

Test section

RESULTS & DISCUSSION

1. Effects of rolling motion

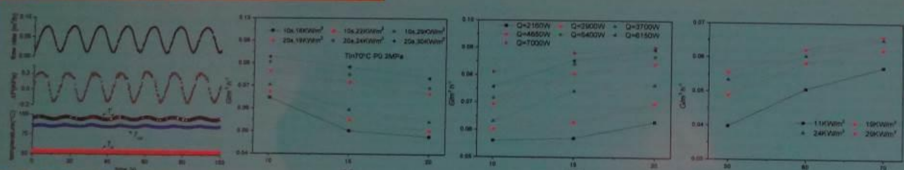

Phenomenon:

a. flow rate, pressure drop, temperature varies periodically as the apparatus rolling

b. With the increase of the amplitude of rolling, the flow rate decreased. With the increase of period of rolling and inlet temperature, the flow rate increased.

2. Characteristics under steady condition

$Nu_b = \lg Re = 1.15\lg\left(\frac{83Nu\cdot Pr_b^{0.11}}{Pr_f^{0.11}[1+(d/L)^{2/3}]}\right)+3.36$ $Nu_s=(0.052Re^{0.75}-14.33)\frac{Pr_f^{0.11}}{Pr_w}\left[1+\left(\frac{d}{L}\right)^{2/3}\right]$

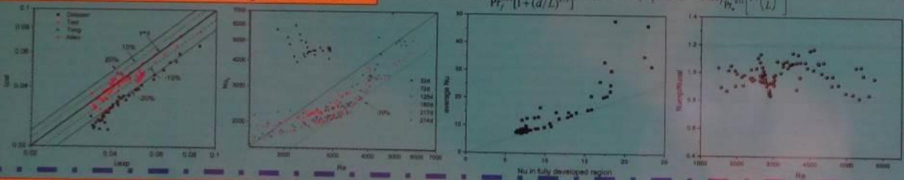

Results:

a. The Test,Allen,Tong methods predict the λ of single phase flow.

b. The average Nu is larger than the Nu in fully developed region.

c. The value of new formula agrees well with the experimental dat.

3. Characteristics under rolling

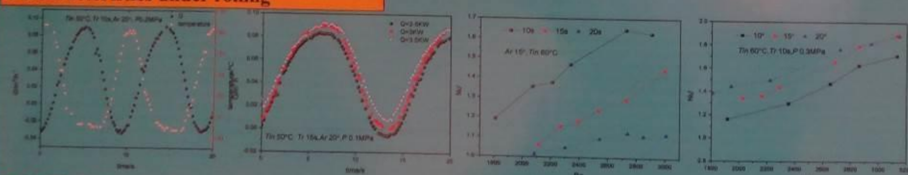

Results:

a. Reverse flow forms that destroy the steady temperature field. The effective method is enhancing the driving force and subdued the additional force, such as increasing the reactor's power.

b. heat transfer of natural circulation under rolling is enhanced. Nu is larger with larger acceleration.

4. FDB of natual circulation

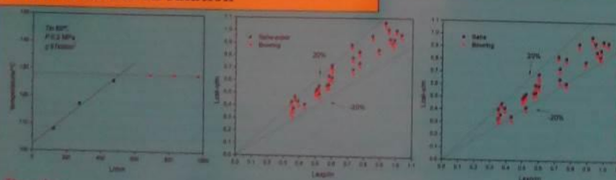

Results:

a. The inflexion of wall temperature is just the point of net vapor generation in subcooled boiling.

b. Saha-zuber model and Bowring models can predict the point of net vapor generation in subcooled boiling

CONCLUSIONS

- The rolling motion can fluctuate the flow and the oscillating frequency of the flow is the same as the rolling frequency.
- For steady condition, Test and Allen methods can be used to predict the λ. The Gnielinski formula can't predict heat transfer coefficient for natural circulation. The result of new formula agrees with the experimental data.
- Rolling reduces the flow of natural circulation. And rolling enhances the heat transfer ability.

Wang Jiangwen

Master Candidate

College of Nuclear Science And Technology
Harbin Engineering University,
Harbin, China.

E-mail: jiangwen15@126.com

Research Fields:
Thermal-hydraulics under ocean conditions

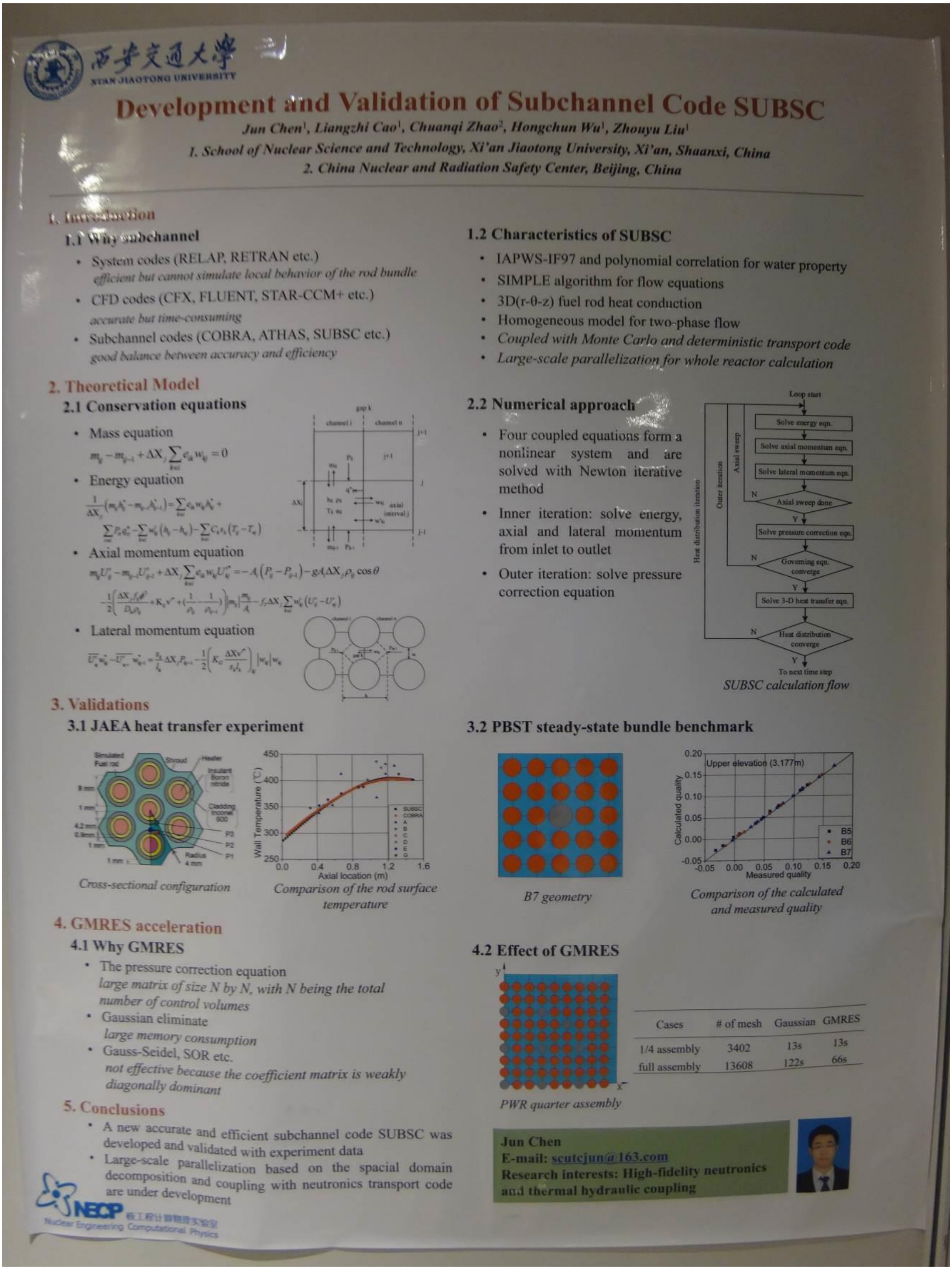

西安交通大學
XI'AN JIAOTONG UNIVERSITY
Development and Validation of Subchannel Code SUBSC
Jun Chen1, Liangzhi Cao1, Chuanqi Zhao2, Hongchun Wu1, Zhouyu Liu1
1. School of Nuclear Science and Technology, Xi'an Jiaotong University, Xi'an, Shaanxi, China
2. China Nuclear and Radiation Safety Center, Beijing, China
1. Introduction
1.1 Why subchannel
System codes (RELAP, RETRAN etc.)
efficient but cannot simulate local behavior of the rod bundle
CFD codes (CFX, FLUENT, STAR-CCM+ etc.)
accurate but time-consuming
Subchannel codes (COBRA, ATHAS, SUBSC etc.)
good balance between accuracy and efficiency
1.2 Characteristics of SUBSC
IAPWS-IF97 and polynomial correlation for water property
SIMPLE algorithm for flow equations
3D(r-θ-z) fuel rod heat conduction
Homogeneous model for two-phase flow
Coupled with Monte Carlo and deterministic transport code
Large-scale parallelization for whole reactor calculation
2. Theoretical Model
2.1 Conservation equations
Mass equation
Energy equation
Axial momentum equation
Lateral momentum equation
2.2 Numerical approach
Four coupled equations form a nonlinear system and are solved with Newton iterative method
Inner iteration: solve energy, axial and lateral momentum from inlet to outlet
Outer iteration: solve pressure correction equation
Loop start
Solve energy eqn.
Solve axial momentum eqn.
Solve lateral momentum eqn.
Axial sweep done
Solve pressure correction eqn.
Governing eqn. converge
Solve 3-D heat transfer eqn.
Heat distribution converge
To next time step
Axial sweep
Outer iteration
Heat distribution iteration
SUBSC calculation flow
3. Validations
3.1 JAEA heat transfer experiment
Cross-sectional configuration
Wall Temperature (°C)
Axial location (m)
Comparison of the rod surface temperature
3.2 PBST steady-state bundle benchmark
B7 geometry
Upper elevation (3.177m)
Calculated quality
Measured quality
Comparison of the calculated and measured quality
4. GMRES acceleration
4.1 Why GMRES
The pressure correction equation
large matrix of size N by N, with N being the total number of control volumes
Gaussian eliminate
large memory consumption
Gauss-Seidel, SOR etc.
not effective because the coefficient matrix is weakly diagonally dominant
4.2 Effect of GMRES
PWR quarter assembly
Cases | # of mesh | Gaussian | GMRES
1/4 assembly | 3402 | 13s | 13s
full assembly | 13608 | 122s | 66s
5. Conclusions
A new accurate and efficient subchannel code SUBSC was developed and validated with experiment data
Large-scale parallelization based on the spacial domain decomposition and coupling with neutronics transport code are under development
Jun Chen
E-mail: scutcjun@163.com
Research interests: High-fidelity neutronics and thermal hydraulic coupling
NECP
Nuclear Engineering Computational Physics

DEVELOPING A CONCEPTUAL DESIGN OF SUCTION-BASED EX-CONTAINMENT RADIOACTIVE RELEASE BARRIER SYSTEM AND DEFINING ITS DESIGN LIMITS

Seong-Woo Kang[a], **Man-Sung Yim**[a*]
[a]Department of Nuclear and Quantum Engineering, Korea Advanced Institute of Science and Technology
291 Daehak-ro, Yuseong-gu, Daejeon 305-701
seongwookang@kaist.ac.kr / msyim@kaist.ac.kr (*Corresponding Author)

1. ABSTRACT

During a typical nuclear power plant severe accident, physical barriers and engineered safety systems are designed to protect the people from the in-containment radiological inventory, called the source term. However, there is no engineered system to prevent the dispersion of the radioactive release if these barriers fail and the radioactivity becomes leaked to the environment. This research proposes a conceptual design of a portable comprehensive engineered safety system that can prevent or reduce the consequences of a severe accident and preliminarily defines its design conditions based on a conservative source term analysis.

2. INTRODUCTION

- After the Fukushima Daiichi nuclear power plant accident, the nuclear industry, regulators, and governments began to review the existing weaknesses of the nuclear power plants and have taken steps to avoid another such accident.
- More safety systems such as Containment Filtered Venting System (CFVS) are being installed around the world to avoid radioactive leakage even in a possible worst-case nuclear power plant (NPP) accident.
- The industry and the regulators also are trying to resolve public anxiety by increasing/improving operator training, NPP regulations, and communication to the public.
- However, the general public's view on the concept of risk differs from that of professional engineers and scientists, and they may not accept the notion that another uncontrolled NPP severe accident will not occur.
- Technologies to mitigate the effects of uncontrolled releases may be necessary, and such technologies are being investigated/developed at KAIST.

3. OBJECTIVE

The purpose of this research is to:
- Develop a conceptual design of the Integrated Portable Suction-Centrifugal Filtration System (IPS-CFS)
- Define its design parameters based on a source term analysis for a possible worst-case nuclear power plant accident

4. PROPOSED DESIGN

① **The suction-arm** is designed with a suction nozzle to collect the radioactive materials without letting them escape to the environment and with a vent line to guide the collected radioactive materials into the treatment compartments of the IPS-CFS.
② **The initial container for the incoming radioactive materials** is designed to cool the radioactive materials to reduce volumetric flow rate and to reduce radioactivity.
③ **The centrifugal filtration device** is chosen to separate the radioactive particles based on particle sizes to further increase treatment capability of the system by designing different filtration compartments for particles with different sizes.
④ **The compartment for absorbed particles in liquid and solid phase** is designed to treat and to contain the separated large particles
⑤ **The compartment for absorbed gas particles** is designed to effectively remove most of the radioactivity before releasing the treated gas into the environment.
⑥ **The transportation device**, most likely in a form of a truck and a trailer that can be controlled remotely, is required for the portability of the IPS-CFS

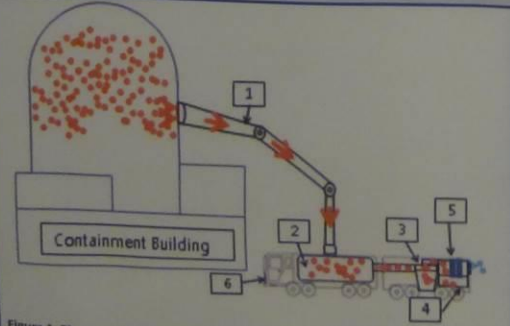

Figure 1. The Concept of the Integrated Portable Suction-Centrifugal Filtration System

5. METHODS

- The source term analysis of the containment rupture scenario from over-pressurization from an extended station blackout (SBO) and a loss of auxiliary feedwater system is simulated for 72 hours
- Following outputs were collected for 72-hours of extended SBO simulation:
  - Mass releases of each fission product (FP) group
  - Temperature, pressure, and density of the gas inside the containment
  - Containment gas mass flow rate to the environment
  - Volumetric flow rate and speed calculated using collected outputs
- Mass release from the MAAP4 simulation is used to estimate the dose rates from volatile/semi-volatile radioactive materials (I, Cs, Te, and Sr), assuming that the activity is directly proportional to the dose rate
- Assuming all radioactive materials are successfully collected by the IPS-CFS, the required decontamination factor to maintain the dose limit to the emergency workers exposed 8 hours a day at 50m away from the source (limit: 250 mSv/y, from US EPA's "Protection Action Guides and Planning Guidance for Radiological Incidents") was calculated.

6. RESULTS

- Due to significant differences in conditions during the depressurization stage (1) and the stable stage (2) as shown in Figure 2, the design limits for the IPS-CFS are drawn for different durations.
- Parameters that may present mechanical design challenges are shown in red in the Table 2.

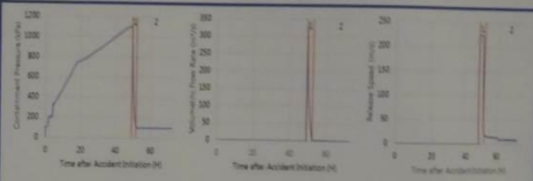

Figure 2. The Containment Pressure and the Radioactive Release Flow Rates after the Accident Initiation

Table 1. The Design Limits for the IPS-CFS for the Different Stages of the Accident (Extended Station Blackout with no Auxiliary Feedwater for 72 Hours)

	Depressurization Stage		Stable Stage	
Time after Release (H)	0~1	1~3	3~5	5~
Duration (H)	1	2	2	Long Term
Temperature (°C)	210	180	180	180
Mass Flow Rate (kg/s)	110	41	1	1
Volumetric Flow Rate (m^3/s)	330	130	5	2
Release Speed (m/s)	230	230	30	15
Decontamination Factor – Iodine	50000	20000	1000	1000
Decontamination Factor - Other Volatile Aerosols	1000	500	100	100

7. CONCLUSIONS

7.1 CONCLUSIONS

- The task of designing a radioactive dispersion system that can successfully prevent such releases through high pressure is very challenging.
- Many conservative assumptions, including the accident scenario, conservative radioactivity dose rate calculations were taken, resulting in very conservative results.
- More source term analyses required to estimate realistic physical realistic source term conditions and the required decontamination factor of the system.

7.2 FUTURE WORK

- More realistic (less conservative) source term analyses that results in radioactive releases
- Feasibility study of the system
- Defining design basis conditions of the system
- Economic analysis of the system
- CFD modeling and simulation of the IPS-CFS during the severe accident conditions

Preparation and properties of Ce based oxide loaded honeycomb catalyst for detritiation

Quanwen Wu, Xiayan Yan, Jingwen Ba, Wenhua Luo,* Daqiao Meng*

Institute of Material Science in China Academy of Engineering Physics

Abstract: In order to prepare a catalyst for both Air Detritiation (AD) and Glove box (some times filled with inert gas) Detritiation (GD), Ce-base oxide ($Ce_{0.7}Zr_{0.3}O_2$, signed as CZ) was used as the support because of its function for oxygen storage. The doping effect of Zr as well as the strong metal-support interaction (SMSI) made the catalyst Pt/CZ feasible for GD with low reduction temperature and high oxygen storage capability (OSC). When coated on honeycomb substrate, the catalyst (Pt/CZ-HC) was also efficient for AD (where the gas-flow rate was always high) because of its low gas resistance and high Pt dispersity. The preparation, properties and detritiation performance of Pt/CZ-HC were introduced in this study.

Background

Tritium safety

Safety

Multi-confinement and
Detritiation System

Air detritiation (ADS);
Vent detritiation (VDS) ;
Glove box deritiation (GDS).

Catalytic oxidation + adsorption;
Metal gas getter.

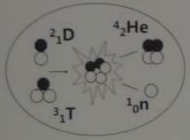

Detritiation → T_2 in → catalyst → T_2O out

Air detritiation → Pt/Al_2O_3

Air and inert atmo. detritiation → Pt/CeO_2, Pt/CZ-HC

Energy from fusion reaction is considered to be potential for future. But the safety especially tritium safety must be seriously considered. Detritiation systems are important parts in fusion facility, for gaseous tritium catalytic oxidation and adsorption is an useful detritiation method. CZ is used as support due to its oxygen storage function, and honeycomb cordierite is used as substrate for its regular structure.

Methods

Preparation of CZ

$Ce(NO_3)_3.6H_2O$
$ZrO(NO_3)_2.H_2O$
{ Sol-gel method / Chemical precipitation } ⇨ Drying (washing) and calcination

Preparation of Pt/CZ-HC

CZ —(Impregnate with $H_2PtCl_6.6H_2O$ solution)→ Pt/CZ —(Milling to slurry)→ Coating on honeycomb substrates

Results

Effect of doped Zr

Table. 1 The speciific surface area of supports

Samples	Calcination temperature (°C)	Specific surface area (m^2/g)
CeO_2	500	56
	700	8.1
	900	7
CZ	500	84
	700	61
	900	11

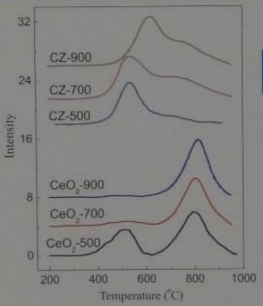

Fig. 1 The TPR profiles for supports

Effect of loaded Pt

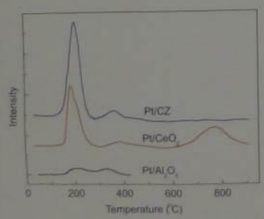

Fig. 2 The TPR profiles for catalysts

Zr → Bulk oxygen ⇩ Increase OSC

Pt → Surface oxygen ⇩ Decrease temper.

⇩ Pt/CZ available for GD

Catalytic performance for Pt/CZ-HC

Table. 2 The catalytic performance under O_2-rich atmosphere

Flow rate ($ml\cdot min^{-1}$)/ space velocity (h^{-1})	Temper. (°C)	H_2 concen. (ppm)	Conv. rate (%)
250/15940	21	2980	100
400/25504	21	3730	100
500/31880	20	5040	100

* Size of catalyst: ϕ8mm×20mm

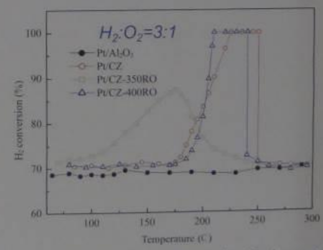

Fig. 3 The catalytic performance under O_2-lean atmosphere

The catalyst shows outstanding catalytic performance for hydrogen oxidation. The H_2 conversion rate is 100% at room temperature when the space velocity is 3.2×10^4 h^{-1} under O_2-rich atmosphere, and is 100% at 200 ℃ when O_2 is deficient. The results indicates the catalyst is useful for both AD and GD.

Conclusions

1. CZ with high redox properties (high OSC and low reduction temperature) was prepared;
2. Pt/CZ-HC was prepared and proved to be useful in both air and glove box detritiation.


A PROLIFERATION RESISTANCE ANALYSIS FOR SODIUM-COOLED FAST BURNER CORE HAVING THORIUM BLANKETS
WuSeung You, Ser Gi Hong
Department of nuclear engineering, Kyunghee university, 1732 Deokyoungdaero, Giheung-gu, Yongin, Gyeonggi-do, 446-701
wsyou87@gmail.com, sergihong@khu.ac.kr
경희대학교
PBNC
Introduction
An advanced SFR burner core concept has been designed using axial thorium blanket to improve performances of the SFR burner core.
The use of Thorium blanket in burner core leads to
-The reduction of burnup reactivity swing due to the breeding of 233U through neutron capture by 232Th.
-The reduction of coolant void worth because of the fact that the η-value increases more slowly with energy for 233U than for 239Pu and 232Th is less fissile than 238U.
However, the use of blanket(thorium or uranium) results in the generation of high fissile concentration material (i.e., 233U) and so the issues of the proliferation resistance are important. And in our previous works, the issues of proliferation resistance associated with the use of thorium blanket have been not addressed.
The objective of this work is to analyze the proliferation resistance of the blanket fuels after discharge from the reactors and to neutronically analyze the advanced SFR burner core using proliferation-resistant blankets.
In analysis of proliferation resistance, the main targets of the discharged blanket fuel in terms of proliferation resistance are
1) Low fissile uranium concentration which satisfies the following condition :
U proliferation index = (233U + 0.6 235U) / U^Total × 100 < 12wt%
2) Larger bare critical mass of plutonium than the plutonium of the reference PWR spent fuel.
3) Higher decay heat from plutonium and 4) Higher spontaneous fission rate from plutonium than from plutonium of the reference PWR spent fuel.
Modeling for Analyzing core performance
Calculations have been performed for analyzing core performance of SFR burner which is a 400MWe Sodium-cooled Fast Reactor and use metallic fuel, TRU-U-10Zr for driver.
The SFR core is designed to generate to 1015.6MWth of power as shown in Fig. 1.
Large central non-fuel regions which consist of B4C shield assemblies and sodium ducts are considered to increase TRU burning rate and to reduce sodium void reactivity.
Table I shows the calculation parameters used in the reference core.
Fig. 2 shows the axial configuration of the reference SFR burner core.
The thorium blanket is loaded in the axially central driver core regions.
We analyzed the effect of different axial blanket in the core performances.
Table I Design parameters for the reference core
Design parameter
Specification
Power (MWe/MWt)
400/1015.6
Number of rods per FA
271
Smear density of fuel
75%
Duct wall thickness (mm)
3.7
Assembly pitch (cm)
16.22
Fig. 1. Configuration of the reference SFR burner core
Table II Composition of external TRU feed from LWR spent fuel
External TRU feed composition 50MWd/kg, 10year cooling from LWR
Fig. 2. Axial configuration of the reference SFR burner core
The depletion analysis was done with REBUS-3 equilibrium model and 9 group cross sections. And we assumed Pyro-reprocessing with 99.9% recovery of TRU and 5% rare earth FP nuclides.
The core physics parameter evaluation was done with DIF3D HEX-Z nodal option and 80group cross section library.
Analysis Results
Analysis of Proliferation Resistance of discharged blanket fuels
The several different blankets are considered by adding depleted uranium(DU) and TRU from LWR spent fuel in order to improve the proliferation resistance of the discharged blankets for our SFR burner cores.
Table III shows comparison of uranium proliferation resistance index
The core having 70Th-30DU blankets has lower U proliferation index than 12wt% but the addition of DU into the axial blanket lead to the production of high quality plutonium(239Pu content of 94wt% in plutonium).
To decrease quality of plutonium, TRUs from LWR spent fuel are added into the blankets.
The core having 65Th-30DU-5TRU blanket has lower fissile Pu contents than that of the PWR spent fuel of 50MWD/kg and zero cooling time (see the last column in Table III) with uranium proliferation index of 10.6%.
Table III Comparison of uranium proliferation resistance index and plutonium compositions of discharged axial blankets from the SFR burner cores
Parameter
Only Thorium
Th-DU 75%-25%
Th-DU 70%-30%
Th-DU-TRU 70%-25%-5%
Th-DU-TRU 65%-30%-5%
Table IV shows comparison of BCM of plutonium compositions of discharged axial blankets.
These BCMs were evaluated by using MCNP6 and blanket compositions are extracted the results of depletion calculations using REBUS-3.
65Th-30DU-5TRU case has higher BCM of 13.46kg than the LWR case
Table V and VI summarize spontaneous fission neutron source (SNS) generation rates and thermal heat generation(TG) rates from the plutonium compositions of the different axial blankets.
The axial blankets of 65wt% thorium and 30wt% DU exceeds the SNS and TG generation rates of the plutonium of the LWR spent fuel due to the high content of Pu-238 and Pu-240. These isotopes give the highest spontaneous fission source and highest heat generation.
Table IV Comparison of BCM of plutonium compositions of discharged axial blankets
Parameter
Th-DU 70-30 22.1MWD/kg
Th-DU-TRU 65-30-5 33.9MWD/kg
PWR U-235(4wt%) 50.0MWD/kg
Pu contents wt%
Table V Comparison of SNS of plutonium compositions of discharged axial blankets
Nuclide
Spontaneous fission source (kg-sec)
Table VI Comparison of SNS of plutonium compositions of discharged axial blankets
Analysis of Proliferation Resistance
Table VII Comparison of performances of the cores having axial different blankets
Conclusion
The parametric study on the blanket composition with addition of DU and TRU showed that it is possible to make the blanket to have higher proliferation resistance in terms of the proliferation resistance indices.
Specifically, discharged spent blanket of 65wt% Th – 30wt% DU – 5wt%LWR spent fuel TRU has higher values of BCM, SNS, TG and U proliferation index than that of PWR discharged fuel.
Also, the core neutronic analysis showed that the SFR burner core using new axial Th-based blankets added with DU and TRU has high proliferation resistance with only slightly degraded performances and reactivity coefficient in comparison with the reference SFR burner core having the axial Th-blanket.
Computational Transport Analysis & Reactor Physics Laboratory

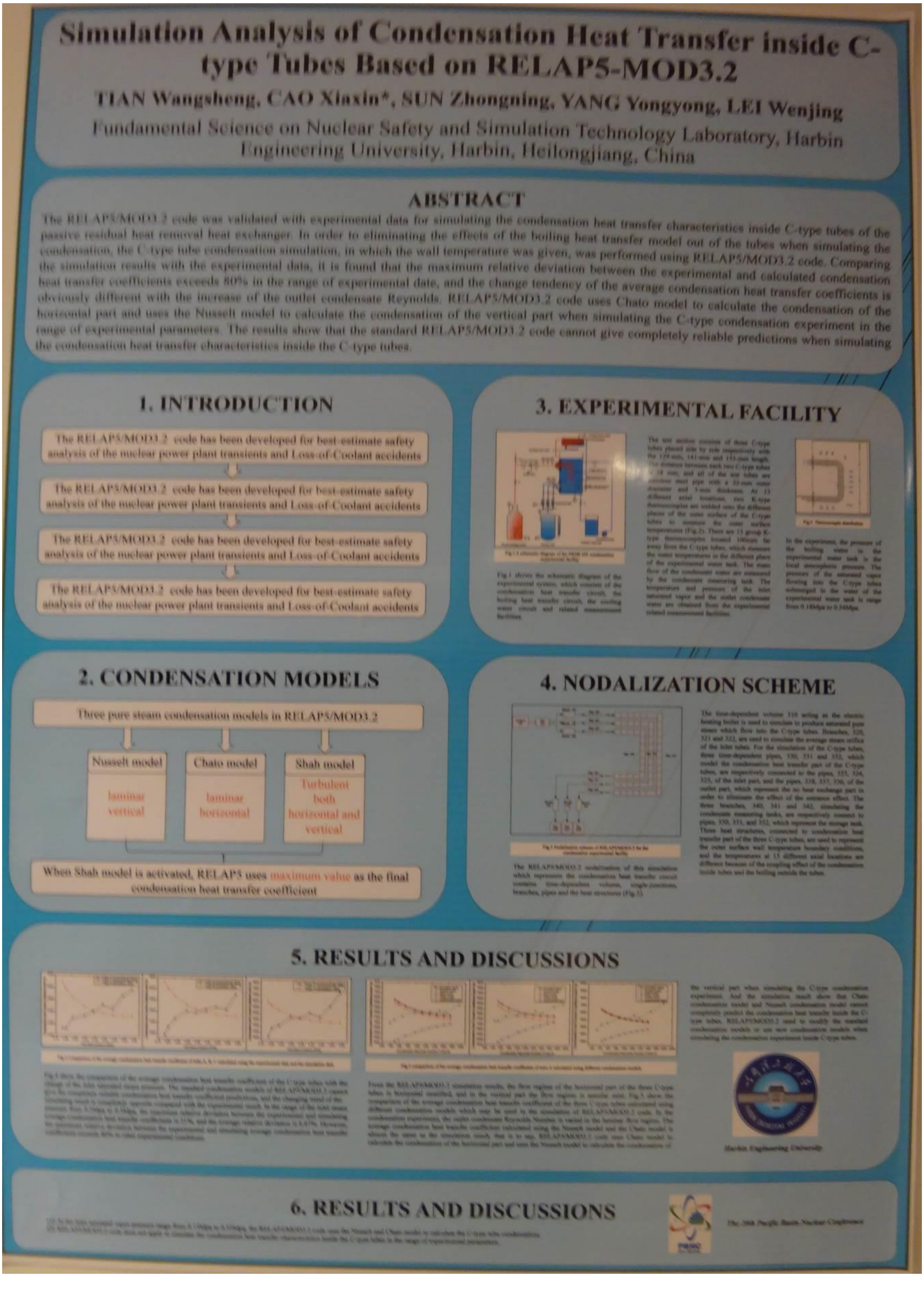
Simulation Analysis of Condensation Heat Transfer inside C-type Tubes Based on RELAP5-MOD3.2
TIAN Wangsheng, CAO Xiaxin*, SUN Zhongning, YANG Yongyong, LEI Wenjing
Fundamental Science on Nuclear Safety and Simulation Technology Laboratory, Harbin Engineering University, Harbin, Heilongjiang, China
ABSTRACT
The RELAP5/MOD3.2 code was validated with experimental data for simulating the condensation heat transfer characteristics inside C-type tubes of the passive residual heat removal heat exchanger. In order to eliminating the effects of the boiling heat transfer model out of the tubes when simulating the condensation, the C-type tube condensation simulation, in which the wall temperature was given, was performed using RELAP5/MOD3.2 code. Comparing the simulation results with the experimental data, it is found that the maximum relative deviation between the experimental and calculated condensation heat transfer coefficients exceeds 80% in the range of experimental date, and the change tendency of the average condensation heat transfer coefficients is obviously different with the increase of the outlet condensate Reynolds. RELAP5/MOD3.2 code uses Chato model to calculate the condensation of the horizontal part and uses the Nusselt model to calculate the condensation of the vertical part when simulating the C-type condensation experiment in the range of experimental parameters. The results show that the standard RELAP5/MOD3.2 code cannot give completely reliable predictions when simulating the condensation heat transfer characteristics inside the C-type tubes.
1. INTRODUCTION
The RELAP5/MOD3.2 code has been developed for best-estimate safety analysis of the nuclear power plant transients and Loss-of-Coolant accidents
The RELAP5/MOD3.2 code has been developed for best-estimate safety analysis of the nuclear power plant transients and Loss-of-Coolant accidents
The RELAP5/MOD3.2 code has been developed for best-estimate safety analysis of the nuclear power plant transients and Loss-of-Coolant accidents
The RELAP5/MOD3.2 code has been developed for best-estimate safety analysis of the nuclear power plant transients and Loss-of-Coolant accidents
3. EXPERIMENTAL FACILITY
2. CONDENSATION MODELS
Three pure steam condensation models in RELAP5/MOD3.2
Nusselt model
laminar vertical
Chato model
laminar horizontal
Shah model
Turbulent both horizontal and vertical
When Shah model is activated, RELAP5 uses maximum value as the final condensation heat transfer coefficient
4. NODALIZATION SCHEME
5. RESULTS AND DISCUSSIONS
Harbin Engineering University
6. RESULTS AND DISCUSSIONS
The 20th Pacific Basin Nuclear Conference

VALIDATION OF THE CROSS-CALIBRATION MULTISPECTRAL INFRARED THERMOGRAPHY IN SURFACE TEMPERATURE MEASUREMENTS

Benjamin Auve[1][2], Alexander Huber[1], Emmanuel Joffrin[1]
[1]Joint European Torus, [2]Tsinghua University, ben.auve@gmail.com

Abstract

The tokamak is nowadays one of the most promising methods to meet today's energy needs without CO2 emissions and radioactive wastes.

A huge undertaking…

Joint European Torus (JET)

International Thermonuclear Experimental Reactor (ITER)

Demonstration Power Plant (DEMO)

… where surface temperatures in-vessel are important parameters to know whether the JET ITER-like walls can withstand the high temperatures.

Introduction

JET's goal : Confine and study the behavior of plasma in conditions approaching those required for a fusion reactor.

In this project, **infrared thermography is essential** to measure surface temperatures on the JET divertor tiles.

But… the environment in vessel is highly contaminated during the operations, so that many contaminants can distort the measuring results on the cameras. Thus, it is essential to re-calibrate the infrared cameras without sending people inside the tokamak.

Solution: A new self-calibrated method which is based on the operation of two or more cameras at different wavelengths is thus introduced.

Methods

- In this work, we compare two methods: the pyrometry method (which needs calibration first) and the cross-calibration.
- All these methods are based on the Planck's law: $L = \frac{c_1}{\lambda^4} \frac{\varepsilon}{\exp\left(\frac{c_2}{\lambda T}\right) - 1}$
- Compared to the pyrometry methods (2 cameras, 1 shot), the **cross-calibration takes 2 shots with 2 cameras** at different temperatures.

	T_1	T_2
λ_1	$DL_{11} = k_1 \frac{c_1}{\lambda_1^4} \frac{\varepsilon_1}{\exp\left(\frac{c_2}{\lambda_1 T_1}\right) - 1}$	$DL_{12} = k_1 \frac{c_1}{\lambda_1^4} \frac{\varepsilon_1}{\exp\left(\frac{c_2}{\lambda_1 T_2}\right) - 1}$
λ_2	$DL_{21} = k_2 \frac{c_1}{\lambda_2^4} \frac{\varepsilon_2}{\exp\left(\frac{c_2}{\lambda_2 T_1}\right) - 1}$	$DL_{22} = k_2 \frac{c_1}{\lambda_2^4} \frac{\varepsilon_2}{\exp\left(\frac{c_2}{\lambda_2 T_2}\right) - 1}$

- The expression of the cross-calibration becomes: $T_2 = \frac{c_2}{\lambda_2 \ln\left(\frac{1 - \frac{DL_{22}}{DL_{21}}}{\left(\frac{DL_{12}}{DL_{11}}\right)^{\lambda_1/\lambda_2} - \frac{DL_{22}}{DL_{21}}}\right)}$

Results

Thanks to the expression above, we measured the sensitivity of the formula:

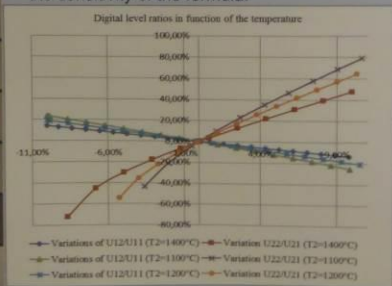

➡ **To get less than 10% error for the temperature, we need less than 2% errors in digital levels accuracy**

With an experimental process (see after), we obtain with a pulse from previous campaigns, a relative error for the temperature: **~4%**

Discussion

- Given that we saw the formula is ill-conditioned, we calibrated the cameras with the blackbody to get the accuracy of the (DL) digital levels. Here are the following steps:
  - Calculation of the neutral density filters;
  - Calculation of the normalized digital levels;
  - Calculation of the calibration coefficients.

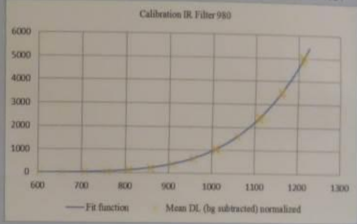

It corresponds to a DL accuracy of ~7.5%.

- Given that 7.5% leads to more than 60% error, we **need to optimize the process**. So that, we used an accurate evaluation of DL on the shots and took into account the variation of emissivity:

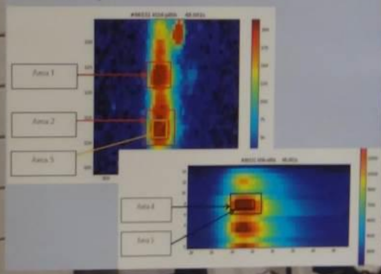

Summary

- The cross-calibration is theoretically feasible…
- …but we need a DL accuracy inferior to 2% to get 10% error for the temperature
- Average accuracy for the DL measurements are about 7.5%
- Thanks to optimizations, we can improve it and make it possible

Literature Cited

F. Meriaudeau, "Real Time Multispectral High Temperature Measurement: Application to control in the industry", Le2i, 2007.

D. Melyukov, C. Sortais, D. Farcage, A. Semerok, P.-Y. Thro and E. Gauthier, "Temperature measurement at large distance of plasma-facing surfaces in fusion reactor by active pyrometry", 10th International Conference on Quantitative InfraRed Thermography, 2010.

C. Pereira, T. Roesgen, S. Walz, S. Airaghi, "The Use of Multispectral Infrared Thermography in Re-entry Vehicles", 11th International Conference on Quantitative InfraRed Thermography, 2012.

[4] T. M. Biewer, D. L. Hillis, M. F. Stamp, K.-D. Zastrow, and JET-EFDA Contributors, "A proposed in-vessel calibration light source for the Joint European Torus", 17th Topical Conference on High Temperature Plasma Diagnostics, 2008.

Disclosure

This work has been done at the Joint European Torus in the Viewing Systems and Thermal Measurements team under the supervision of Dr. Alexander Huber and Dr. Emmanuel Joffrin.

Everything has been reviewed by Pr. Sun Jun at the Institute of Nuclear and New Energy Technology, Tsinghua University.

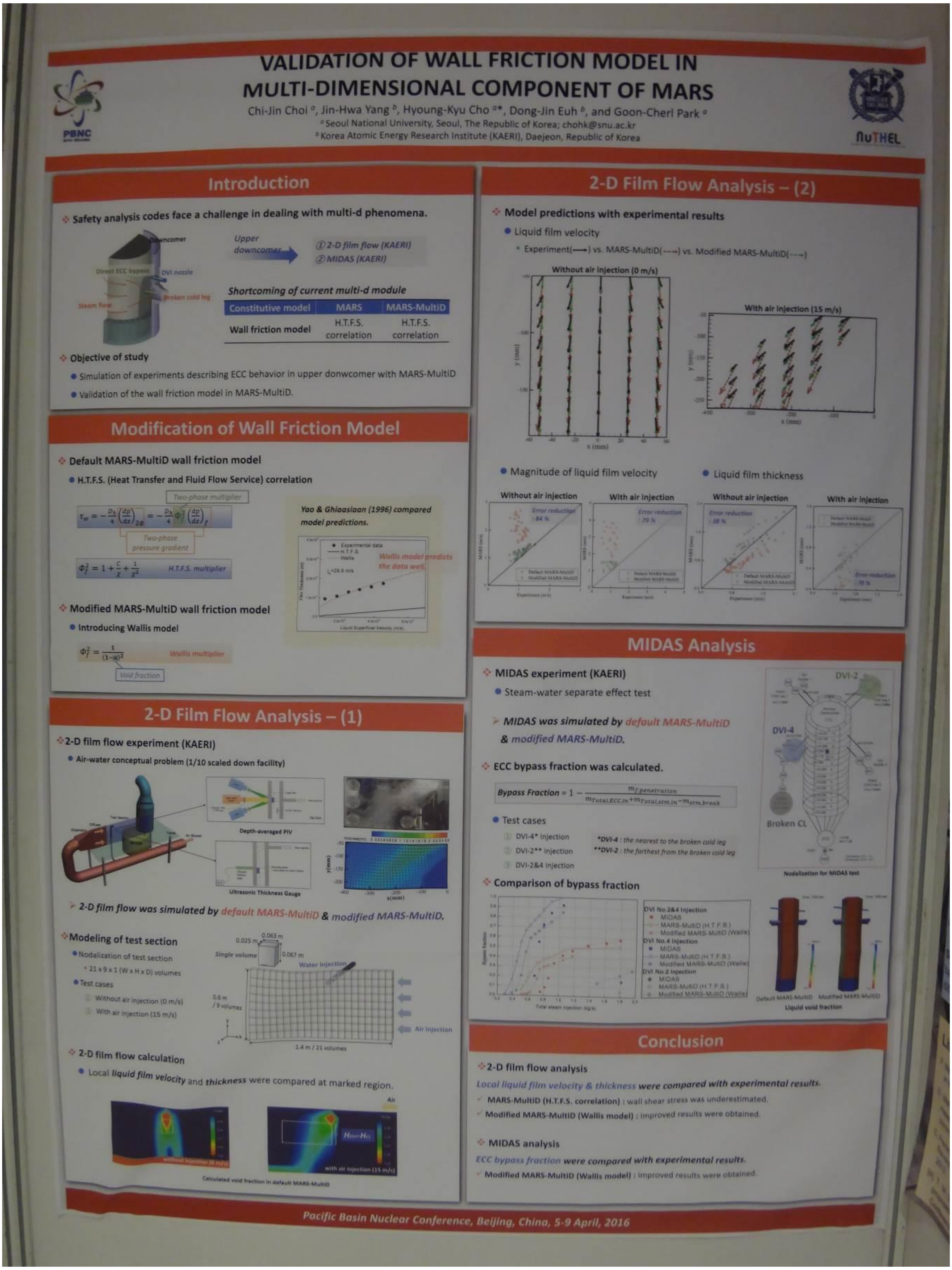
VALIDATION OF WALL FRICTION MODEL IN MULTI-DIMENSIONAL COMPONENT OF MARS
Chi-Jin Choi a, Jin-Hwa Yang b, Hyoung-Kyu Cho a*, Dong-Jin Euh b, and Goon-Cherl Park a
a Seoul National University, Seoul, The Republic of Korea; chohk@snu.ac.kr
b Korea Atomic Energy Research Institute (KAERI), Daejeon, Republic of Korea
Introduction
Safety analysis codes face a challenge in dealing with multi-d phenomena.
Upper downcomer
① 2-D film flow (KAERI)
② MIDAS (KAERI)
Shortcoming of current multi-d module
Constitutive model | MARS | MARS-MultiD
Wall friction model | H.T.F.S. correlation | H.T.F.S. correlation
Objective of study
Simulation of experiments describing ECC behavior in upper donwcomer with MARS-MultiD
Validation of the wall friction model in MARS-MultiD.
Modification of Wall Friction Model
Default MARS-MultiD wall friction model
H.T.F.S. (Heat Transfer and Fluid Flow Service) correlation
Two-phase multiplier
Two-phase pressure gradient
H.T.F.S. multiplier
Yao & Ghiaasiaan (1996) compared model predictions.
Wallis model predicts the data well.
Modified MARS-MultiD wall friction model
Introducing Wallis model
Wallis multiplier
Void fraction
2-D Film Flow Analysis – (1)
2-D film flow experiment (KAERI)
Air-water conceptual problem (1/10 scaled down facility)
Depth-averaged PIV
Ultrasonic Thickness Gauge
2-D film flow was simulated by default MARS-MultiD & modified MARS-MultiD.
Modeling of test section
Nodalization of test section
21 x 9 x 1 (W x H x D) volumes
Test cases
Without air injection (0 m/s)
With air injection (15 m/s)
Single volume
Water injection
Air injection
1.4 m / 21 volumes
2-D film flow calculation
Local liquid film velocity and thickness were compared at marked region.
Calculated void fraction in default MARS-MultiD
2-D Film Flow Analysis – (2)
Model predictions with experimental results
Liquid film velocity
Without air injection (0 m/s)
With air injection (15 m/s)
Magnitude of liquid film velocity
Liquid film thickness
Without air injection
With air injection
MIDAS Analysis
MIDAS experiment (KAERI)
Steam-water separate effect test
MIDAS was simulated by default MARS-MultiD & modified MARS-MultiD.
ECC bypass fraction was calculated.
Test cases
DVI-4* injection
DVI-2** injection
DVI-2&4 injection
*DVI-4 : the nearest to the broken cold leg
**DVI-2 : the farthest from the broken cold leg
Comparison of bypass fraction
Nodalization for MIDAS test
Liquid void fraction
Conclusion
2-D film flow analysis
Local liquid film velocity & thickness were compared with experimental results.
MARS-MultiD (H.T.F.S. correlation) : wall shear stress was underestimated.
Modified MARS-MultiD (Wallis model) : improved results were obtained.
MIDAS analysis
ECC bypass fraction were compared with experimental results.
Modified MARS-MultiD (Wallis model) : improved results were obtained.
Pacific Basin Nuclear Conference, Beijing, China, 5-9 April, 2016

中国工程物理研究院 CHINA ACADEMY OF ENGINEERING PHYSICS

Institute of Materials

Research on Reaction Kinetics of Pt-Pd Catalysts Supported on Porous Stainless Steel Plate

CHEN Zhijiang, JIANG Ting, and GAO Bo*

China Academy of Engineering Physics

1. Abstract

Accident at Fukushima Daiichi Nuclear Power Station has emphasized the importance of mitigation of hydrogen during accidental conditions in nuclear power plant. Passive autocatalytic recombiner (PAR) is considered as one of the best solutions to deal with the problem because of its passive operation for hydrogen removal. Here we report development of porous stainless steel (PSS) plate supported Pt-Pd bimetallic catalysts prepared by electroless deposition route. We developed 5 kinds of catalyst plates with different Pt-Pd proportion. The kinetic treatment of the reaction data was carried out to calculate the reaction rate, temperature rise and apparent activation energy for hydrogen-oxygen recombination on these catalysts.

2. Experimental

The Pt-Pd bimetallic catalysts were prepared by electroless deposition strategy. First, stainless steel filter plates with an average 10 μm pore size were immersed with dilute hydrochloric acid, in order to remove the oxidation on the surface. Then the plates were immersed in H_2PtCl_6 solution or $PdCl_2$ solution or mixed H_2PtCl_6-$PdCl_2$ solution, with little hydrochloric acid to prevent precipitation of noble metal. With the different proportion of H_2PtO_3 solution and $PdCl_2$ solution, we made 5 different catalytic plates: (1) pure Pt, (2) Pt:Pd=4:1(mole ratio), (3) Pt:Pd=1:1, (4) Pt:Pd=1:4, (5) pure Pd.

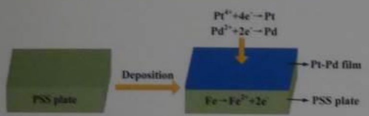

Fig. 1 Illustrative representation of the preparation of the Pt-Pd bimetallic film supported on PSS plate

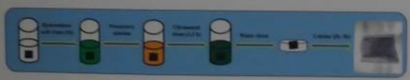

Fig. 2 Preparation process of the Pt-Pd bimetallic catalyst plates

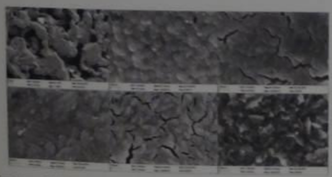

Fig. 3 SEM images of (a) blank PSS, (b) pure Pt, (c) Pt:Pd=4:1, (d) Pt:Pd=1:1, (e) Pt:Pd=1:4, (f) pure Pd

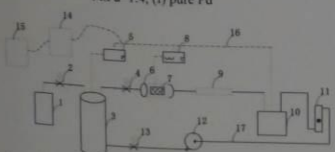

Fig. 4 Block diagram representing the experimental setup for catalytic activity evaluation. 1- hydrogen gas cylinder, 3-mixing vessel, 6-stainless steel reactor, 12-air circulating pump, 5-pressure gauge, 7-catalyst plates, 8-thermocouple, 10-hydrogen monitor, 2,4,13-valve,9-drying tube, 11-rotary flowmeter, 17-gas pipeline, 14-PC machine, 15-date acquisition instrument

3. Result and discussion

Time required for 50% conversion ($t_{1/2}$) and maximum temperature attained (T_{max}) for different catalysts is enlisted in Fig. 5. The $t_{1/2}$ and T_{max} observed for pure Pt catalyst are 445°K and 81 s, while that of pure Pd catalyst are 467°K and 29 s. The total trend is that if the catalyst have a higher ratio of Pd, it will reach a higher temperature by a shorter time.

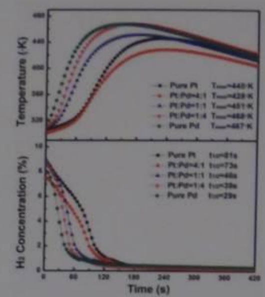

Fig. 5 Variation of $t_{1/2}$ and T_{max} obtained for different samples for initial hydrogen concentration of approximate 8% in air.

Fig. 6 depicts how we get the data of apparent activation energy, take the sample of Pt:Pd=4:1 as an example, from the typical catalytic activity data show in Fig. 5. We choose the data between the two dotted lines, in which region the H_2 concentration decrease rapidly and the temperature rise rapidly. We can obtain the apparent activation energy E_a from the Arrhenius equation:

$$\ln k = -\frac{E_a}{RT} + \ln A$$

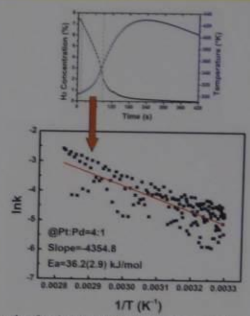

Fig. 6 Arrhenius plot for the determination of apparent kinetics: ln*k* versus 1/*T* (Pt:Pd=4:1).

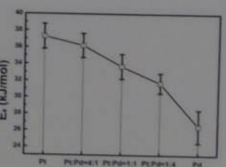

Fig. 7 The apparent activation energy of 5 different catalysts

4. Conclusion

Platinum-palladium bimetallic catalysts supported on porous stainless steel plates were successfully prepared by a modified electroless deposition route. To compare the behavior, especially of the 5 different catalysts, we built an experimental setup for catalytic activity evaluation. The experiment indicate that if the catalyst has a higher proportion of Pd, the catalyst will has a higher rate of hydrogen mitigation, accordingly a small apparent activation energy.

5. Acknowledgement

We gratefully acknowledge the financial support provided by National Natural Science Foundation of China (21406212), National Magnetic Confinement Fusion Energy Research Project (2015GB109003), the Applied Basic Research Programs of Science and Technology Department of Sichuan Province, China (2015JY0041).

*Corresponding author. E-mail address: gaobo@caep.cn, Tel: +86-0816-3620721

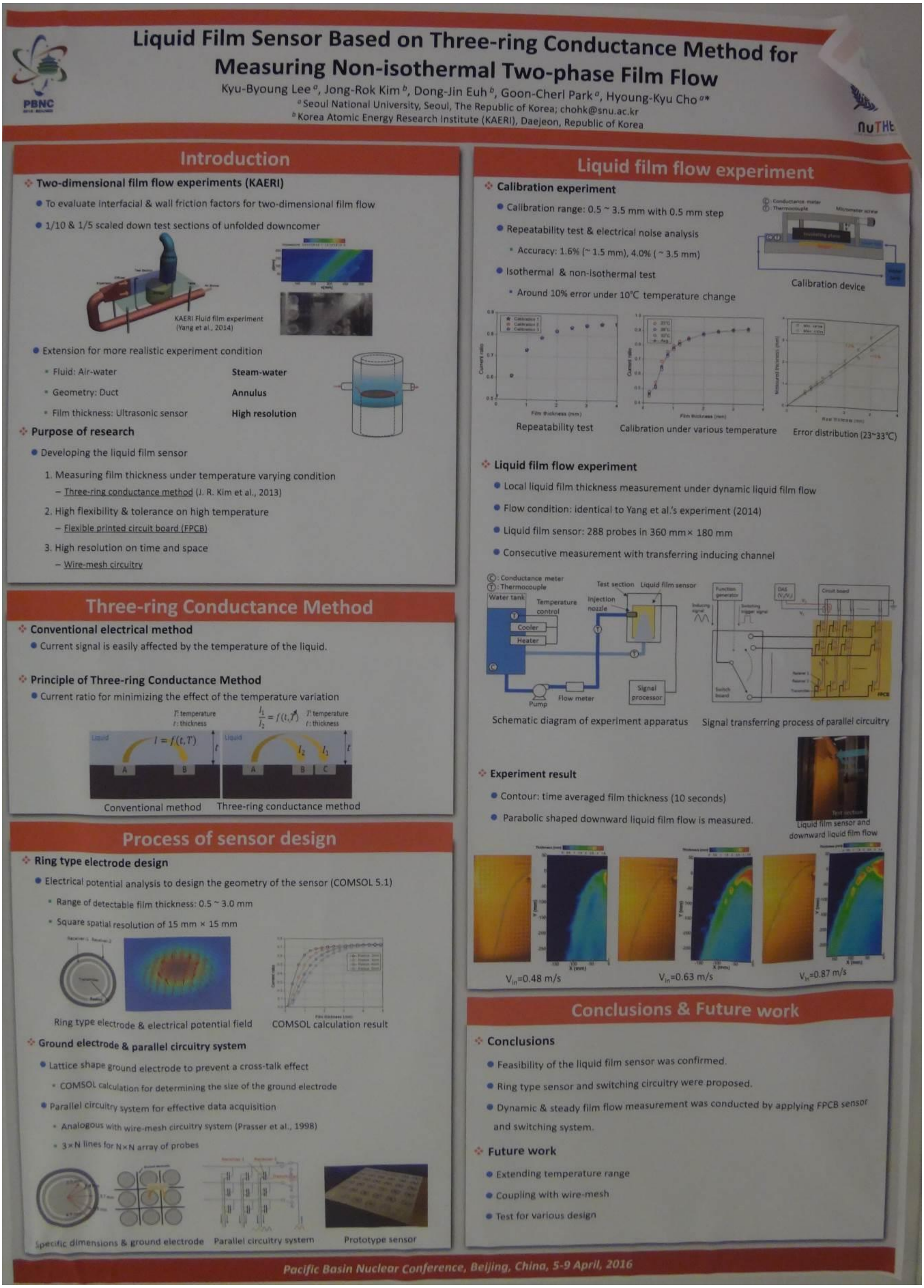

Liquid Film Sensor Based on Three-ring Conductance Method for Measuring Non-isothermal Two-phase Film Flow

Kyu-Byoung Lee[a], Jong-Rok Kim[b], Dong-Jin Euh[b], Goon-Cherl Park[a], Hyoung-Kyu Cho[a]*

[a] Seoul National University, Seoul, The Republic of Korea; chohk@snu.ac.kr

[b] Korea Atomic Energy Research Institute (KAERI), Daejeon, Republic of Korea

Introduction

- Two-dimensional film flow experiments (KAERI)
  - To evaluate interfacial & wall friction factors for two-dimensional film flow
  - 1/10 & 1/5 scaled down test sections of unfolded downcomer

KAERI Fluid film experiment (Yang et al., 2014)

- Extension for more realistic experiment condition
  - Fluid: Air-water → **Steam-water**
  - Geometry: Duct → **Annulus**
  - Film thickness: Ultrasonic sensor → **High resolution**
- Purpose of research
  - Developing the liquid film sensor
    1. Measuring film thickness under temperature varying condition
       – Three-ring conductance method (J. R. Kim et al., 2013)
    2. High flexibility & tolerance on high temperature
       – Flexible printed circuit board (FPCB)
    3. High resolution on time and space
       – Wire-mesh circuitry

Three-ring Conductance Method

- Conventional electrical method
  - Current signal is easily affected by the temperature of the liquid.
- Principle of Three-ring Conductance Method
  - Current ratio for minimizing the effect of the temperature variation

$I = f(t,T)$ (T: temperature, t: thickness)

$\frac{I_2}{I_1} = f(t, \cancel{T})$ (T: temperature, t: thickness)

Conventional method / Three-ring conductance method

Process of sensor design

- Ring type electrode design
  - Electrical potential analysis to design the geometry of the sensor (COMSOL 5.1)
    - Range of detectable film thickness: 0.5 ~ 3.0 mm
    - Square spatial resolution of 15 mm × 15 mm

Ring type electrode & electrical potential field / COMSOL calculation result

- Ground electrode & parallel circuitry system
  - Lattice shape ground electrode to prevent a cross-talk effect
    - COMSOL calculation for determining the size of the ground electrode
  - Parallel circuitry system for effective data acquisition
    - Analogous with wire-mesh circuitry system (Prasser et al., 1998)
    - 3×N lines for N×N array of probes

Specific dimensions & ground electrode / Parallel circuitry system / Prototype sensor

Liquid film flow experiment

- Calibration experiment
  - Calibration range: 0.5 ~ 3.5 mm with 0.5 mm step
  - Repeatability test & electrical noise analysis
    - Accuracy: 1.6% (~ 1.5 mm), 4.0% (~ 3.5 mm)
  - Isothermal & non-isothermal test
    - Around 10% error under 10°C temperature change

Calibration device

Repeatability test / Calibration under various temperature / Error distribution (23~33°C)

- Liquid film flow experiment
  - Local liquid film thickness measurement under dynamic liquid film flow
  - Flow condition: identical to Yang et al.'s experiment (2014)
  - Liquid film sensor: 288 probes in 360 mm× 180 mm
  - Consecutive measurement with transferring inducing channel

Schematic diagram of experiment apparatus / Signal transferring process of parallel circuitry

- Experiment result
  - Contour: time averaged film thickness (10 seconds)
  - Parabolic shaped downward liquid film flow is measured.

Liquid film sensor and downward liquid film flow

V_{in}=0.48 m/s / V_{in}=0.63 m/s / V_{in}=0.87 m/s

Conclusions & Future work

- Conclusions
  - Feasibility of the liquid film sensor was confirmed.
  - Ring type sensor and switching circuitry were proposed.
  - Dynamic & steady film flow measurement was conducted by applying FPCB sensor and switching system.
- Future work
  - Extending temperature range
  - Coupling with wire-mesh
  - Test for various design

Pacific Basin Nuclear Conference, Beijing, China, 5-9 April, 2016

University of Science and Technology of China (USTC)

Track 11. Student program

20th PBNC 2015

Neutronics Characteristics Study of Conceptual Space Heat-pipe Cooled Fast Reactor Core

Hui Zhao, Hongli Chen, Chong Chen, Qin Zeng, Haoran Zhang

School of Nuclear Science and Technology , University of Science and Technology of China, Hefei, Anhui, 230026, China

E-mail: huizhao9@mail.ustc.edu.cn, Web: http://en.snst.ustc.edu.cn

ABSTRACT :With the continuous development of space exploration activity, the demand for space energy is increasing. Energy supply has become an very important guarantee for the normal operation of all kinds of space equipment. Therefore, the high-power and long-life space nuclear reactor, which can be operated automatically and not be affected by environment, becomes a very important choice for space energy system. In this paper, a space fast reactor core design scheme based on a integrated structure which combines the nuclear fuel rods and the central cooling heat-pipes was proposed initially. The fuel rod is a regular hexagonal prism, and the evaporator section of the heat-pipe is placed in the central hole of the fuel rod. The control of the reactor depends on six control drums in the side of the reflector. The neutronics characteristics of the reactor core were studied. The reactor core design scheme was calculated and analyzed through the establishment of the core calculation models by means of MCNP. The main dimensions and physical parameters of the reactor core were given, and the critical reactivity, power distribution and burnup of the reactor core was obtained. The fuel filling rate was improved because of the compact layout of the design scheme, which led to a reduction of the critical mass and the core volume of the reactor. At the same time, the use of structural material also decreased. As a result, the total mass of the core reduced. An increasing relative density of heat-pipe arrangement could avoid the problem generated by the failure of single heat pipe effectively. Consequently, it has high safety and good reliability.

Keywords: Space nuclear reactor, Heat-pipe, Reactivity, Power distribution, Burnup

1. Introduction

With the development and implementation of deep space exploration programs in the world, the space base construction on the moon or other planets will be of great scientific, military and political value in the future. Energy supply and management has become an important guarantee for the normal and stable operation of the bases.

At present, the high-power and long-life space nuclear reactor, which can be operated stably and reliably, has become a very important and advanced research topic in the design and research of space base energy system.

2. Design concept and scheme

The electrical power required by the space base is generally between 10~100kW, and the lifetime need to be more than 5 years[3]. This paper puts forward a design scheme of space nuclear reactor core with the thermal power of 1000 kW, the electric power of 60kW, the static thermoelectric conversion efficiency of 6%, the lifetime more than 10 years.

- **Core type:** Fast reactor.
- **Cooling method:** Heat-pipe cooling.
- **Thermoelectric conversion method:** Static thermocouple conversion.

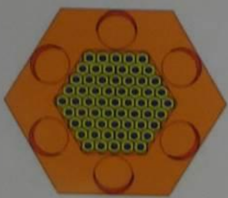

Fig.1 Core structure model

Table 1. Main design parameters of space nuclear reactor core

Parameters	Design value	Parameters	Design value
Core thermal power	1000 kWth	Margin of the active area	440mm
Thermoelectric conversion efficiency	6%	Active area height	600mm
Electric power	60kWe	Margin of the active area	244mm
Core lifetime	10 years	The thickness of the reflector	Side face: 98mm Upper/Lower face: 70mm
Number of fuel rods	61	The diameter of control drums	90mm
Number of control drums	6	The height of control drums	600mm
Total height of the core	740mm	Absorber size	Crescent, most thickness is 10mm

3. Neutronics analyses

3.1 Reactivity analysis

- The total reactivity was negative.
- In case of an accident, even if half of the control drums got stuck outside, The rest of the drums could also achieve a safe shutdown.
- The core was divided into two modules in the design to avoid the critical risk effectively when the core fall into the water.

Table 2. Critical parameters of space nuclear reactor

Calculation state	k_{eff}	Δk/k/%
Initial state(cold state)	1.02835	2.75
Initial state(Hot state)	1.02444	2.39
Put into all control drums	0.91447	-9.36
Put into five control drums	0.93302	-7.18
Put into three control drums	0.96660	-3.46
1/2 core fall into the water	0.87303	-14.5
Full power operation for ten years	1.00773	0.76

3.2 Power distribution

- The average power of each fuel rod was 16.39kW.
- The maximum power peaking factor of the core was 1.09 with a power of 17.8kW.
- With a failure of one heat-pipe, the power need to transfer from the six heat-pipes around. It will increase a factor of 1/6 to be 20.6kW
- The maximum heat transfer limit of the heat-pipe is more than 25kW.
- So the heat could be brought out effectively

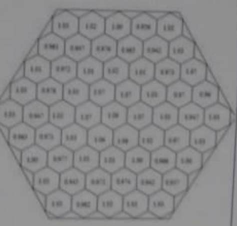

Fig. 2 Relative power distribution of the core

3.3 Burnup analysis

After running for 3600 days (about 10 years), the absolute burnup of the core reaches 14.48GWd/MTU and the keff was gradually reduced to 1.0073 .

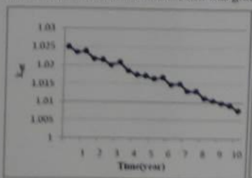

Fig. 3 The keff of the core during operation

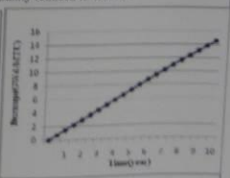

Fig. 4 Burnup of the core during operation

4. Conclusion

This design based on a integrated structure which combines the nuclear fuel rods and the central cooling heat-pipes has some advantages:

- ✓ The fuel rods could be arranged closely to improve the fuel filling ratio
- ✓ The critical mass and volume reduce significantly, which is conducive to flatten power distribution.
- ✓ The total mass of the core is decreased and it is helpful for the launch.
- ✓ The smaller volume improves neutron leakage rate, which makes the core easier to control.

NQe
Department of Nuclear & Quantum Engineering

A STUDY OF APPLICATION OF A FIRE TRUCK FOR THE SEVERE ACCIDENT OUTSIDE THE NUCLEAR POWER PLANT

KAIST
한국과학기술원

JongWook Go[a], Irfan Younus[a] and Man-Sung Yim[a]
[a]Department of Nuclear and Quantum Engineering, Korea Advanced Institute of Science and Technology
gowe1234@kaist.ac.kr / msyim@kaist.ac.kr

ABSTRACT: When a severe accident occurs, large amounts of radioactive materials may be released. This possibility also increases the public's fear of nuclear power plants (NPPs). Also, the economic impact of a severe accident can be huge as shown in the Fukushima accidents. Given these considerations, technologies to prevent the dispersal of these materials are desirable. Technologies to capture the radioactive materials have been studied. One example of such technology is to use spray. Use of spray inside nuclear power plant has been developed with the use of alkaline water. In this study, we propose to use spray technology to collect the materials released outside the plant. Although there are various types of liquids that can be used with spray technology this study investigated water spray as the baseline technology and because sea and fresh water are readably available near NPPs. To deploy the spray technology, use of a fire engine specially equipped with a "boom" that can be extended to reach higher locations was envisioned in this study. The capability of the spray technology was analyzed through Computational Fluid Dynamics (CFD) analysis. By using a CFD modeling-based simulation, this study investigated the effectiveness of fire engine mounted sprays in reducing dispersion of radioactive materials in a severe accident. In particular the study examined the role of the distance of the spray nozzle from the containment and nozzle angle, to improve the effectiveness of the spray.

1. Introduction

1.1 Background

After the Fukushima accident,

- Public fear of nuclear energy has increased,
- Importance of nuclear safety has resurfaced,
- Regulations regarding the operation of nuclear power plants have been revised and are stricter.

For improved safety of Nuclear Power Plants (NPPs),

- Containment Filtered Vented System (CFVS) are planed to be installed
- Other safety equipment has been installed
- But there are no alternatives to preventing radioactive materials from spreading into the environment once they are discharged from the containment building

1.2 Purpose of this study

Purposes

- To investigate engineering applications of spray technology to mitigate severe accident consequence
- Develop a numerical method for the spray technology
- Analyze dependency of spray efficiency on different spray angles and distances

1.3 Approach for this study

- ANSYS CFX, one of the computational fluid dynamics (CFD) tools, was used to develop a numerical model replicating the use of spray technology around the containment building
- Mathematical equations were used to modeled the spray scrubbers
- Numerical simulations were performed at 1/50th scale of a typical containment building. These results will be used to validate future experimental results from testing on a physical model.

2. Mathematical modeling

- The number of solid particles removed by a single droplet

$$N_c = \eta_s \frac{\pi d_p^2}{4} |U_s - U_p| \frac{N_s}{dV}$$

- N_c: The number of solid particles removed by a single droplet
- d_p: The diameter of a droplet
- N_s: The number of solid particles in an element volume
- dV: An element volume
- $|U_s-U_p|$: relative velocity between solid particles and a droplet

- Inertial impaction parameter

$$\psi = \frac{\rho_F d_s^2 |U_F - U_P|}{9 \mu d_P}$$

- d_s: The diameter of a solid particle
- μ: The viscosity of fluid around a droplet
- ρ_F: The density of fluid around a droplet
- $|U_F-U_P|$: relative velocity between fluid around a droplet and the droplet

- Removal efficiency of solid particles in the system

$$\eta_{total} = 1 - \frac{m_{out,solid}}{m_{in,solid}}$$

- Removal efficiency of solid particles by a single droplet

$$\eta_s = \left(\frac{\psi}{\psi + 0.7}\right)^2$$

3. Numerical simulation

3.1 Flow state

The Eulerian approach

- The Eulerian approach was used to solve for the behaviors of air and TiO_2 dust
- Steady state and incompressible flow were assumed
- The k- ε model was used for turbulence
- The diameter of TiO_2 dust was assumed as 10 μm
- Instead of radioactive substances, TiO_2 was used in order to compare numerical results with future experimental results.

The Lagrangian approach

- The Lagrangian approach was used for calculating the behavior of the sprayed water particles
- The Cascade Atomization and Breakup (CAB) model was used for modeling the breakup of water particles
- Gravity and drag were considered as external forces

3.2 Mesh

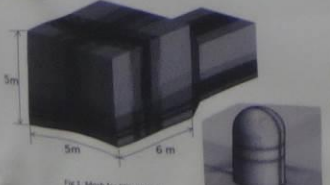

Fig 1. Mesh for CFD analysis

- The number of elements
  - About 2,400,000
- The shape of mesh elements
  - Hexahedron
- Size of this setup
  - 1/50th of a NPP
  - Lab-scale

3.3 Boundary conditions

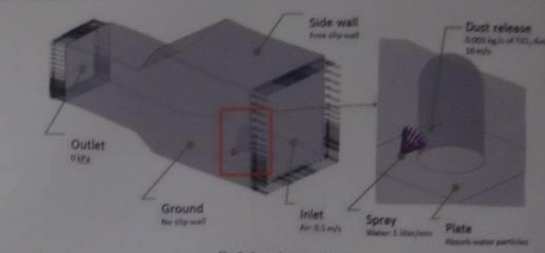

Fig 2. Boundary conditions

3.4 Spray injection

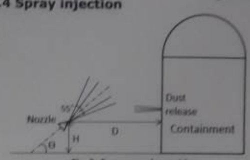

Fig 3. Spray nozzle position

- Position
  - D: 60 cm, 90 cm
  - H: 40 cm (Maximum of Firetruck)
  - θ: 30°, 45°, 60°
- Nozzle
  - Flow rate: 1 liter/min
  - Spray angle: 55°
  - Spray shape: Cone
- Dust release
  - Diameter: 6 mm
  - Height: 60 cm
  - Mass flow rate(TiO_2): 0.001 kg/s
  - Velocity: 10 m/s

4. Results & discussions

4.1 Mesh dependency test

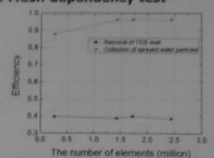

Fig 4. The results for mesh dependency tests

- Removal efficiency of TiO_2 dust is almost independent of the number of mesh elements.
- Collection efficiency of sprayed water particles is converged after about 1.4 million elements.
- If the number of elements exceed 1.4 million, the error from the mesh becomes small.
- In this study, the number of elements is about 2.4 million. Therefore, the results are reasonable.

4.2 Results

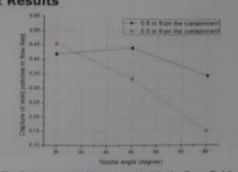

Fig 5. Removal efficiency of TiO_2 in flow field

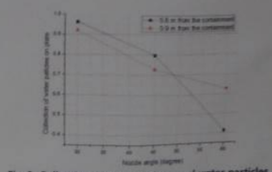

Fig 6. Collection efficiency of sprayed water particles on plate

- These results indicate that if spray is close to the containment, the removal efficiency is larger in general.
- At 0.6 m from the containment, the maximum value of removal efficiency is about 45% at a 45 degree nozzle angle, but collection efficiency of water particles is lower than achieved at 30 degrees.
- Comparing these results, the best nozzle angle is 30 degree.

5. Summary

5.1 Summary

1) Capture efficiency of TiO_2 dust by water particles is the highest at 60 cm from the containment and at a 45° nozzle angle because the volume covered by water particles are larger than other cases. So many of the TiO_2 dust particles are captured in this volume (Figure 5).
2) Collection efficiency of water particles on plate (Figure 6) is the highest at 60 cm from the containment with a 30° nozzle angle. This is because most of the water particles collide on the containment surface (Figure 6).
3) If the capture efficiency of TiO_2 dust and the collection efficiency of water particles are considered together, the best case is at 60 cm from the containment with a 30° nozzle angle (Figures 5 and 6).
4) In this study, the numerical model used to analyzing a venturi scrubber, was applied for calculating dust removal efficiency in an external flow. The approach appears appropriate when analyzing the performance of a spray system installed on a fire truck.

5.2 Future work

1) Consideration of the effect of varying the diameter of TiO_2 dust and other capturing mechanisms.
2) Development of experimental data to validate the computational simulation model.
3) Analysis of the effect of water film on the containment wall.
4) Optimization of the use of spray technology mounted on a specialized fire truck.

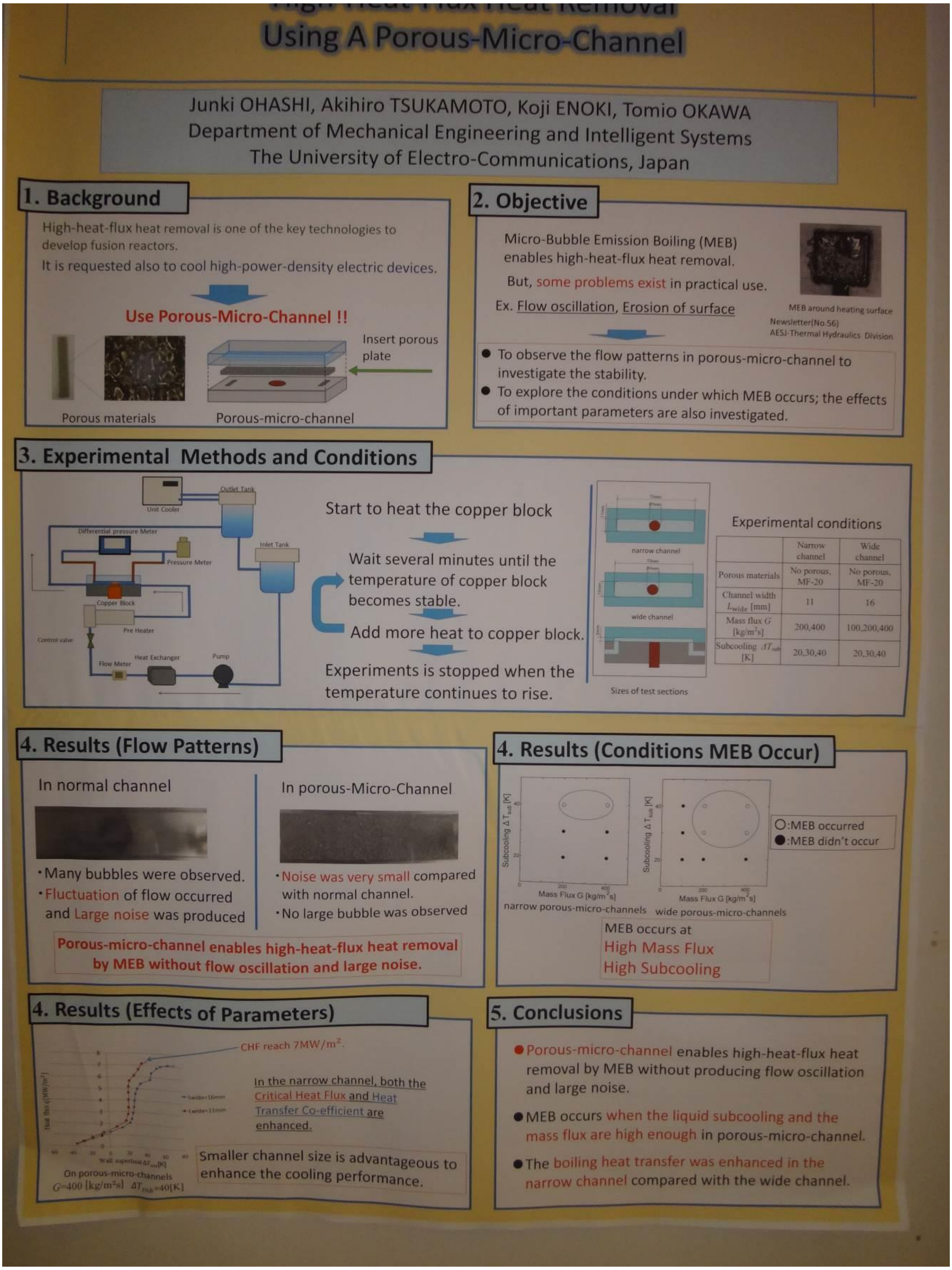
Using A Porous-Micro-Channel
Junki OHASHI, Akihiro TSUKAMOTO, Koji ENOKI, Tomio OKAWA
Department of Mechanical Engineering and Intelligent Systems
The University of Electro-Communications, Japan
1. Background
High-heat-flux heat removal is one of the key technologies to develop fusion reactors.
It is requested also to cool high-power-density electric devices.
Use Porous-Micro-Channel !!
Insert porous plate
Porous materials
Porous-micro-channel
2. Objective
Micro-Bubble Emission Boiling (MEB) enables high-heat-flux heat removal.
But, some problems exist in practical use.
Ex. Flow oscillation, Erosion of surface
MEB around heating surface
Newsletter(No.56)
AESJ-Thermal Hydraulics Division
To observe the flow patterns in porous-micro-channel to investigate the stability.
To explore the conditions under which MEB occurs; the effects of important parameters are also investigated.
3. Experimental Methods and Conditions
Unit Cooler
Outlet Tank
Differential pressure Meter
Pressure Meter
Inlet Tank
Copper Block
Pre Heater
Control valve
Flow Meter
Heat Exchanger
Pump
Start to heat the copper block
Wait several minutes until the temperature of copper block becomes stable.
Add more heat to copper block.
Experiments is stopped when the temperature continues to rise.
narrow channel
wide channel
Sizes of test sections
Experimental conditions
Narrow channel
Wide channel
Porous materials
No porous, MF-20
No porous, MF-20
Channel width L_{wide} [mm]
11
16
Mass flux G [kg/m^{2}s]
200,400
100,200,400
Subcooling ΔT_{sub} [K]
20,30,40
20,30,40
4. Results (Flow Patterns)
In normal channel
In porous-Micro-Channel
・Many bubbles were observed.
・Fluctuation of flow occurred and Large noise was produced
・Noise was very small compared with normal channel.
・No large bubble was observed
Porous-micro-channel enables high-heat-flux heat removal by MEB without flow oscillation and large noise.
4. Results (Conditions MEB Occur)
Subcooling ΔT_{sub} [K]
Mass Flux G [kg/m^{2}s]
narrow porous-micro-channels
wide porous-micro-channels
○:MEB occurred
●:MEB didn't occur
MEB occurs at
High Mass Flux
High Subcooling
4. Results (Effects of Parameters)
CHF reach 7MW/m^2.
In the narrow channel, both the Critical Heat Flux and Heat Transfer Co-efficient are enhanced.
On porous-micro-channels
G=400 [kg/m^{2}s] ΔT_{sub}=40[K]
Smaller channel size is advantageous to enhance the cooling performance.
5. Conclusions
Porous-micro-channel enables high-heat-flux heat removal by MEB without producing flow oscillation and large noise.
MEB occurs when the liquid subcooling and the mass flux are high enough in porous-micro-channel.
The boiling heat transfer was enhanced in the narrow channel compared with the wide channel.

DYNAMIC MODEL DEVELOPMENT OF A SODIUM-HEATED STEAM GENERATOR

Zi Wang, Peiwei Sun, Jianmin Zhang
Xi'an Jiaotong University, Xi'an,
Shaanxi, 710049, China
Email:510356793@qq.com

西安交通大學

ABSTRACT

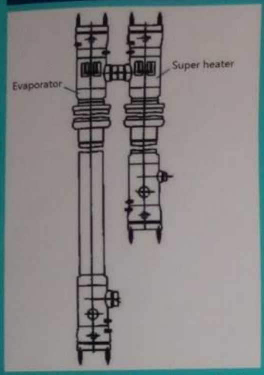

Steam generator of sodium-cooled fast reactor is a critical component. Its operation and control is important to safety of the reactor. Therefore, it is necessary to develop its dynamic model and investigate its dynamics. Moving boundary method was applied to derive its dynamic model. Steady-state calculation was performed and the results agreed well with the design parameter and those from references. Transient simulations was carried out by introducing disturbances. The dynamics of the steam temperature and sodium outlet steam were analyzed.

INTRODUCTION

In China, the fast reactor plays a very important role in the strategic plan of using nuclear energy. China National Nuclear Corporation is developing the industrial scale prototype fast reactor CFR600 .Because CFR600 is still under conceptual design and its design of steam generator follows that of the China experiment fast reactor (CEFR). The investigations on CEFR steam generator will be valuable references to the development and research of CFR600 steam generator.

METHODS

For the moving boundary model, according to the phase state and thermal hydraulic characteristics of water/steam, the tube is divided into four regions along the flow direction. The thermal-hydraulic model is derived the based on the conversation equations and Leinitz theorem. A computer program is developed for thermal-hydraulic model of CEFR steam generator and Gear method is applied to solve the stiff ordinary differential equations.

INPUT DATA

Input data	Values
Feedwater mass flow rate /kg/s	13.35
Number of tubes in evaporator	187
Number of tubes in superheater	138
Feedwater temperature /℃	190.0
Sodium outlet temperature /℃	310.0
Steam outlet pressure /MPa	14.0
Tube length in evaporator /m	12.24
Tube length in superheater /m	7.72
Sodium mass flow rate /kg/s	137.98

MODEL VERIFICATION

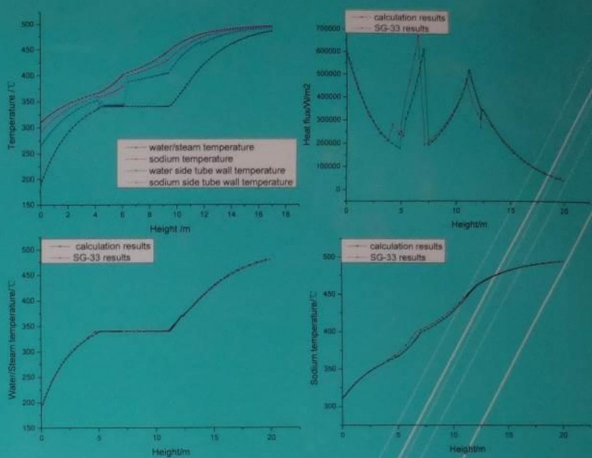

TRANSIENT RESULTS

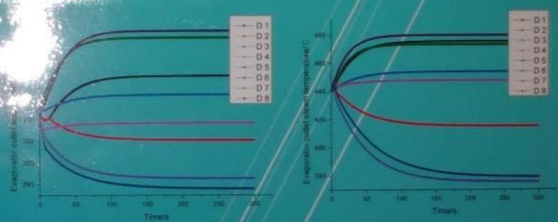

D 1 is 10℃ step increase in the sodium inlet temperature;
D 2 is 10℃ step decrease in the sodium inlet temperature;
D 3 is 10% step increase in the sodium flow rate;
D 4 is 10% step decrease in the sodium flow rate;
D 5 is 10℃ step increase the feedwater inlet temperature;
D 6 is 10℃ step decrease the feedwater inlet temperature;
D 7 is 10% step increase the feedwater flow rate;
D 8 is 10% step decrease the feedwater flow rate.

CONCLUSIONS

The steady-state results are compared with those of SG-33 and CEFR design. The results show a favorably good agreement with the Russian results.
Transient simulations are carried out by introducing disturbances. The responses are reasonable in theory. The most significant influence on the steam outlet temperature and the sodium outlet temperature is from the feedwater flow rate.
The moving boundary model can predict the dynamic behavior of the CEFR steam generator with high accuracy and stability. The numerical method adopted can be directly applied to the model of the CFR600 steam generator. The dynamics obtained for CEFR are also valuable for CFR600.

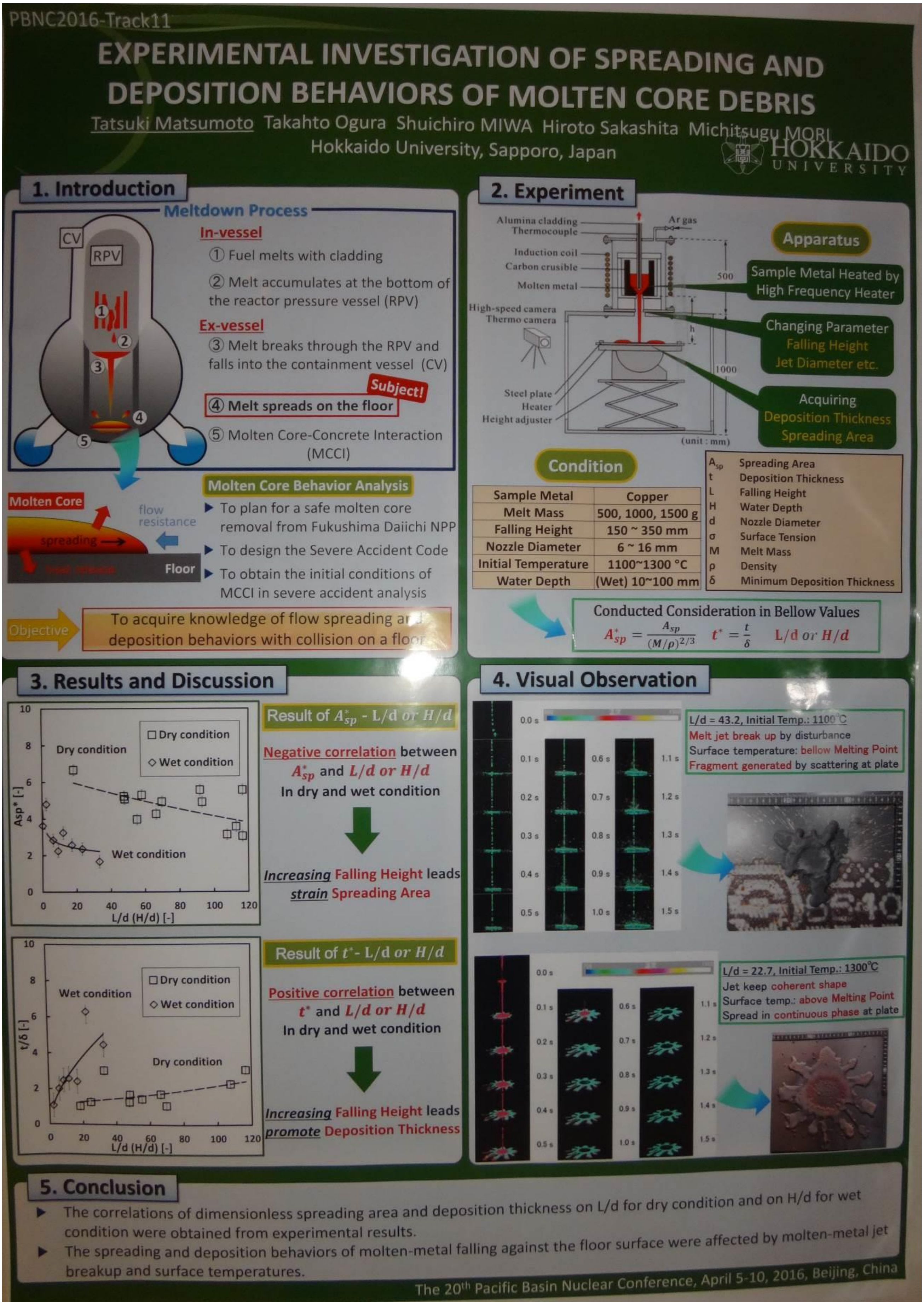
PBNC2016-Track11
EXPERIMENTAL INVESTIGATION OF SPREADING AND DEPOSITION BEHAVIORS OF MOLTEN CORE DEBRIS
Tatsuki Matsumoto Takahto Ogura Shuichiro MIWA Hiroto Sakashita Michitsugu MORI
Hokkaido University, Sapporo, Japan
HOKKAIDO UNIVERSITY
1. Introduction
Meltdown Process
CV
RPV
In-vessel
① Fuel melts with cladding
② Melt accumulates at the bottom of the reactor pressure vessel (RPV)
Ex-vessel
③ Melt breaks through the RPV and falls into the containment vessel (CV)
Subject!
④ Melt spreads on the floor
⑤ Molten Core-Concrete Interaction (MCCI)
Molten Core
flow resistance
spreading
Floor
Molten Core Behavior Analysis
To plan for a safe molten core removal from Fukushima Daiichi NPP
To design the Severe Accident Code
To obtain the initial conditions of MCCI in severe accident analysis
Objective
To acquire knowledge of flow spreading and deposition behaviors with collision on a floor
2. Experiment
Alumina cladding
Thermocouple
Ar gas
Induction coil
Carbon crusible
Molten metal
High-speed camera
Thermo camera
Steel plate
Heater
Height adjuster
500
1000
h
(unit : mm)
Apparatus
Sample Metal Heated by High Frequency Heater
Changing Parameter
Falling Height
Jet Diameter etc.
Acquiring
Deposition Thickness
Spreading Area
Condition
Sample Metal | Copper
Melt Mass | 500, 1000, 1500 g
Falling Height | 150 ~ 350 mm
Nozzle Diameter | 6 ~ 16 mm
Initial Temperature | 1100~1300 °C
Water Depth | (Wet) 10~100 mm
A_sp Spreading Area
t Deposition Thickness
L Falling Height
H Water Depth
d Nozzle Diameter
σ Surface Tension
M Melt Mass
ρ Density
δ Minimum Deposition Thickness
Conducted Consideration in Bellow Values
$A_{sp}^{*} = \frac{A_{sp}}{(M/\rho)^{2/3}}$ $t^{*} = \frac{t}{\delta}$ L/d or H/d
3. Results and Discussion
Dry condition
Wet condition
Asp* [-]
L/d (H/d) [-]
Result of A_{sp}^{*} - L/d or H/d
Negative correlation between A_{sp}^{*} and L/d or H/d
In dry and wet condition
Increasing Falling Height leads strain Spreading Area
t/δ [-]
Result of t^{*} - L/d or H/d
Positive correlation between t^{*} and L/d or H/d
In dry and wet condition
Increasing Falling Height leads promote Deposition Thickness
4. Visual Observation
L/d = 43.2, Initial Temp.: 1100 °C
Melt jet break up by disturbance
Surface temperature: bellow Melting Point
Fragment generated by scattering at plate
L/d = 22.7, Initial Temp.: 1300°C
Jet keep coherent shape
Surface temp.: above Melting Point
Spread in continuous phase at plate
5. Conclusion
The correlations of dimensionless spreading area and deposition thickness on L/d for dry condition and on H/d for wet condition were obtained from experimental results.
The spreading and deposition behaviors of molten-metal falling against the floor surface were affected by molten-metal jet breakup and surface temperatures.
The 20th Pacific Basin Nuclear Conference, April 5-10, 2016, Beijing, China

POWER OPTIMIZATION OF STEAM GENERATORS UNDER FAULT CONDITIONS

Huasong Cao, Peiwei Sun, Jianmin Zhang
Xi'an Jiaotong University, Xi'an, Shaanxi, 710049, China
Email: caohuasong@stu.xjtu.edu.cn

Abstract

The helical coiled once-though steam generator of IRIS is chosen as a research object. A steady-state thermal-hydraulic model of the steam generator of IRIS is developed. Sensitivity analysis is performed to investigate the influences on the thermal power from the steam generator key operation parameters. Feedwater flow rate and average coolant temperature are selected as optimized variables and the thermal power is chosen as the objective function. The constraints on the tube temperature, reactor outlet temperature and reactor inlet temperature are chosen as limits. Polynomial fit algorithm is applied to derive their relationship. The maximum thermal power is found by solving the fitted polynomial under the fault conditions. The thermal power is 30.1% larger than which without optimization. Finally hybrid algorithm is proposed as an alternate method for further study.

Introduction

Steam generator is critical equipment between the primary and secondary loops. The steam generator (SG) of IRIS is a helical-coil tube bundle SG with the primary fluid outside the tubes. There are eight SG modules located in the annular space between the core barrel and the reactor vessel . Each SG module mainly consists of a central inner column. The tube coils are 1.64 m in diameter. Each SG has 656 tubes. The tubes are connected to the vertical sides of the lower feedwater header and the upper steam header .

Methods

1.Build a thermal-hydraulic steady-state model of steam generator;
2. Sensitivity analysis to investigate the influences on the thermal power from the steam generator key operation parameters ;
3. Power optimization with polynomial fit algorithm and hybrid algorithm.

Results

1.The steady-state results

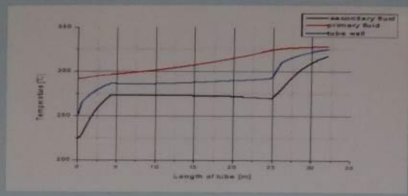

Temperature distribution along the tube

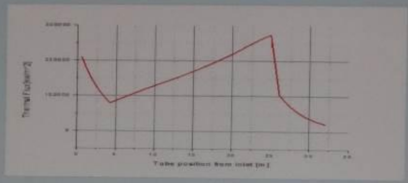

Heat flux distribution along the tube

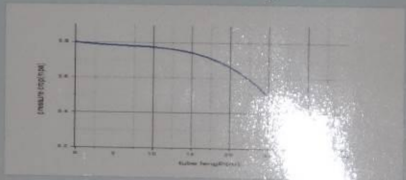

Pressure drop distribution along the tube

2. Sensitivity analysis

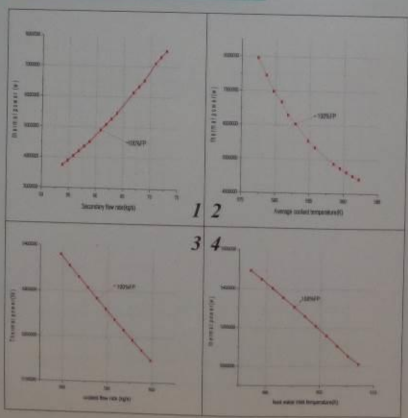

Fig.1 the thermal power at different feedwater flow rates
Fig. 2 thermal power at different average coolant temperature
Fig. 3 the thermal power at different coolant flow rates
Fig. 4 the thermal power at different feed water inlet temperature

3.The result of Polynomial fit algorithm

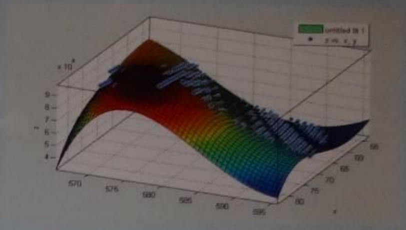

Three-dimensional simulation diagram

The results of optimization

Methods	Feedwater flow rate	Coolant average temperature	Thermal Power
Poly Optimization	70.85(kg/s)	304.15(° C)	787.48(MW)
Without optimization	62.85(kg/s)	309.75(° C)	550.47(MW)

The results of limits

Parameters	Calculated result	Range
Reactor outlet temperature/° C	323.49	300~330
Reactor inlet temperature/° C	284.78	270~300
Tube temperature/° C	291.23	<400

Conclusions

1. A steady-state thermal-hydraulic model of the steam generator of IRIS is developed. The results are compared with those obtained from Relap5 and it is proved the model is accurate enough for further study of the power optimization.
2. Sensitivity analysis is performed to investigate the influences on the thermal power from the steam generator key operation parameters.
3. A fitted polynomial is derived from the data with different the feedwater flow rate and the average coolant temperature. The maximum thermal power is found by solving the fitted polynomial under the fault conditions. The thermal power is 30.1% larger than which without optimization.
4. For further study, hybrid algorithm is proposed to extend the optimization for more general cases.

附件九：大會排程與相關行政資訊：

2016 年 4 月 5 日	17:30-21:30	大會現場註冊
2016 年 4 月 5 日	18:30-21:30	招待會
2016 年 4 月 6 日	07:30-08:30	大會現場註冊
2016 年 4 月 6 日	09:00-12:00	開幕式及全體大會
2016 年 4 月 6 日	13:30-17:00	全體大會
2016 年 4 月 7 日	09:00-12:00	各專題平行會場/ 大會論壇
2016 年 4 月 7 日	13:30-17:00	各專題平行會場/ 大會論壇
2016 年 4 月 8 日	09:00-12:00	各專題平行會場/ 大會論壇
2016 年 4 月 8 日	13:30-17:00	各專題平行會場/ 大會論壇
2016 年 4 月 8 日	17:30-20:00	閉幕式及晚宴
2016 年 4 月 9 日	09:00-12:00	各專題平行會場/ 大會論壇

各專題主席名單：

專題	姓 名	工作單位	職 務
1	信天民	中國核電工程有限公司 北京核工程研究設計院	常務副總工 院長
2	張　濤	中核核電運行管理有限公司	總經理
3	荊春寧	中國核電工程有限公司北京核工程研究設計院	副院長
4	鄧國清	中國核電工程有限公司北京核工程研究設計院	副院長

5	李　明	中國核電工程有限公司	採購部主任
6	葉國安	中國原子能科學研究院	副院長
7	宋丹戎	中國核動力研究設計院	設計總師
8	胡光耀	中國廣核集團	新聞發言人
9	淩曉哲	中核集團財務公司	副總經理
10	何作祥	中國醫學科學院阜外心血管病醫院	研究員
11	於溯源	清華大學	教授

大會工作語言：英語。大會期間將安排中-英同聲傳譯。

大會主辦單位：

中國核學會

中國核工業集團公司

國家核電技術公司

中國廣核集團有限公司

中國核工業建設集團公司

技術支援單位：

中國核電工程有限公司

大會組織機構：

名譽主席—Honorary chair

大會主席—Conference Chairperson

指導委員會—Conference Steering Committee

--國際指導委員會

--國內指導委員會

技術委員會—Technical Program Committee

組織委員會—Conference Organization Committee

大會主席及各委員會主席：

大會名譽主席:

大會主席：孫勤，中國核工業集團公司董事長

指導委員會主席：

雷增光，中國核工業集團公司總工程師、中國核學會副理事長

Mary Holland Limbach,太平洋核理事會理事長

技術委員會主席：薑巨集，中國核電工程有限公司副總經理

組織委員會主席：李冠興，中國核學會理事長

組織委員會常務副主席：申立新，中國核學會副秘書長